Published as NIST SP 250-83

NIST Special Publication 250-83

Calibration of Hygrometers with the Hybrid Humidity Generator

C.W. Meyer
J.T. Hodges
P.H. Huang
W.W. Miller
D.C. Ripple
G.E. Scace

Thermometry Group
Process Measurements Division
Chemical Science and Technology Laboratory

December 2008

U.S. Department of Commerce
Carlos M. Gutierrez, Secretary

National Institute of Standards and Technology
Patrick Gallagher, Deputy Director

ABSTRACT

We describe here the calibration of customer hygrometers using a new humidity generator that has been commissioned at the National Institute of Standards and Technology. The NIST Hybrid Humidity Generator (HHG) generates frost/dew points from –70 °C to +85 °C (mole fractions from 1×10^{-6} to 0.57) using calibration gas flows up to 150 standard liters per minute. The HHG combines the two-pressure and divided-flow humidity generation techniques (hence the name "hybrid"). The centerpiece of the HHG is a heat exchanger/saturator that is immersed in a temperature-controlled bath stable to within 1 mK. For dew/frost point temperatures above –15 °C, the two-pressure principle is employed. For frost points at or below –15 °C, the water-vapor/air mixture is produced by mixing metered streams of moist air produced by the two-pressure method with purified, dry air. In this special publication, we describe the design of the generator. We also describe a series of performance and validation tests on the HHG and use the results of these to construct an uncertainty budget for the generator when used in two-pressure mode and when used in the divided-flow mode. These tests include measurements of temperature gradients and pressure stability in the generator under various operating conditions, and comparison of the humidity generated by the HHG to that generated or measured by the other NIST humidity standards. For dew/frost point temperatures, the uncertainty budget yields a total expanded uncertainty ($k = 2$) of less than 0.025 °C for dew/frost point temperatures above –60 °C. For mole fraction, the budget yields a total expanded relative uncertainty of less than 0.2 % for mole fractions above 2×10^{-5}.

KEY WORDS: humidity; generator; standards; saturator; calibration; hygrometer; water vapor.

National Institute of Standards and Technology Special Publication 250-83
Natl. Inst. Stand. Technol. Spec. Publ. 250-83, 48 pages (December 2008)
CODEN: NSPUE2

Calibration of Hygrometers with the Hybrid Humidity Generator

Table of Contents

1. Overview of the Calibration Service

The NIST Hybrid Humidity Generator [1,2] provides calibration services for a variety of humidity–measuring instruments. Calibrations are performed by subjecting the instrument under test to air with an accurately known moisture content produced by the generator. The calibration system described here does not currently include a test chamber (a chamber in which the humid air is directed and where the temperature and pressure are sufficiently constant and uniform). At this time, hygrometers requiring a test chamber for calibration must be calibrated using the NIST 2-P Mark II Generator. The calibrations may be performed using humidity definitions of dew/frost point, relative humidity, mole fraction, or mass ratio. For the case of relative humidity calibrations, a separate calibration of the instrument's external temperature probe is performed by means of comparison against a standard thermometer. The instruments and ranges of calibration include but are not restricted to:

1. Chilled-Mirror Hygrometers, calibrated at customer-specified points over the dew/frost range of –70 °C to +85 °C, or alternatively over the relative-humidity range 5% to 100% for temperatures between −45 °C and 85 °.

2. Aluminum-oxide Hygrometers, calibrated at customer-specified points over the dew/frost range of –70 °C to +85 °C.

3. Electrolytic Hygrometers, calibrated at customer-specified points over a volume-ratio range of 10^{-6} to the upper limit of the hygrometer.

4. Cavity Ring-Down Hygrometers, calibrated at customer-specified points over a volume-ratio range of 10^{-6} to the upper limit of the hygrometer.

Customers should consult the web addresses http://www.nist.gov/thermometry and http://ts.nist.gov/MeasurementServices/Calibrations/Humidity.cfm to find the most current information regarding calibration fees and technical contacts. The Thermometry Group follows the policies and procedures described in the NIST Calibration Services Users Guide, which can be found at these web addresses: http://ts.nist.gov/MeasurementServices/Calibrations/policy.cfm http://ts.nist.gov/MeasurementServices/Calibrations/domestic.cfm and http://ts.nist.gov/MeasurementServices/Calibrations/foreign.cfm.
These web pages give instructions for ordering a calibration for domestic and foreign customers. They discuss: a) customer inquiries, b) pre-arrangements and scheduling, c) purchase orders, d) shipping, insurance, and risk of loss, and e) turnaround time.

2. Principle of Operation

Generation of gas with an accurately known moisture content starts with saturating the gas with water at a known temperature and pressure. Controlled saturation is accomplished by flowing a stream of the gas over a layer of water with a constant, uniform temperature until the gas is in

thermodynamic equilibrium with the water. Ideally, the pressure of the gas is constant and pressure gradients within the gas are negligible. The mole fraction x of water vapor in the gas is then calculated using the equation

$$x = \frac{e(T_s)}{P_s} f(T_s, P_s) \quad (1)$$

Here, T_s and P_s are the temperature and pressure of the gas and water in the saturator, and $e(T_s)$ is the water vapor pressure at T_s, as calculated by [3,4]. The enhancement factor $f(T_s, P_s)$ reflects departures from ideal solution behaviour and non-ideal gas effects [5]. When P_s is approximately at ambient pressure, the generator is said to operate in one-pressure (1-P) mode.

At a given value of T_s, two methods can be used to lower the humidity while still knowing its value accurately: the two-pressure (2-P) technique and the divided-flow method. The hybrid humidity generator (HHG) is capable of using these two methods separately or together (hence the name *hybrid*). The two-pressure technique [6] involves saturating the gas at an elevated pressure and afterwards expanding the gas down to ambient pressure. The divided-flow method [6] involves diluting the saturated gas with dry gas using precisely metered streams of gas. Such a technique allows generation of arbitrarily low humidity values while operating the saturator at convenient temperatures. When performing hygrometer calibrations, the HHG operates in 1-P or 2-P mode for mole fractions greater than or equal to 1.6×10^{-3} (a frost point of −15 °C). The HHG uses the divided flow method for mole fractions less than this value.

3. Humidity Definitions

The HHG generates humidity by the definition of mole fraction, but calibrations are also performed for other definitions, though they may require additional measurements.

The dew point temperature T_{DP} is defined as the temperature (for a given mole fraction x and gas pressure P_c) at which liquid water and water vapor are in equilibrium. Here, the subscript "c" in P_c refers to the chamber in which the dew point is being determined, (although the gas, if air, is often in an open environment). Experimentally, determination of T_{DP} requires the additional measurement of P_c. Once P_c has been determined, T_{DP} is obtained by iteratively solving the equation

$$x = \frac{e(T_{DP})}{P_c} f(T_{DP}, P_c) \,. \quad (2)$$

While Eq. 2 is structurally similar to Eq. 1, $T_{DP} = T_s$ only when $P_c = P_s$. Similarly, the frost point temperature T_{FP} is given by

$$x = \frac{e_i(T_{FP})}{P_c} f(T_{FP}, P_c) \,, \quad (3)$$

where e_i is the saturated vapor pressure for ice, as calculated by [7,8].
Relative humidity is defined by

$$RH \equiv \frac{e_p}{e(T_c)} = \frac{xP_c}{e(T_c) f(T_c, P_c)} \quad (4)$$

where e_p is the partial pressure of the water vapor in the air and T_c is the air temperature in the chamber or location of interest. Experimentally, determination of *RH* requires the additional measurements of P_c and T_c. Chilled-mirror hygrometers that determine *RH* do so by directly measuring T_{DP} using the chilled mirror, measuring T_c with an external thermometer, and calculating *RH* using Eqs. 2−3 while assuming $f(T_{DP}, P_c) \cong f(T_c, P_c)$.

The mass ratio *r* is equal to the ratio of water mass to air mass in a given volume of gas, and is related to the mole fraction by

$$r = \frac{m_w}{m_a} \frac{x}{1-x} = 0.62196 \frac{x}{1-x}, \quad (5)$$

where m_w = 18.015268 g/mol [9] and m_a = 28.96546 g/mol [10] are the molar masses of water and air, respectively.

4. Generator Design

A schematic representation of the layout of the HHG is shown in Figure 1 for a) the 2-P mode and b) the divided-flow mode. The system involves a dry gas source, a two-pressure saturation system and (for divided-flow mode) a dilution system. The components of the HHG are described below.

4.1. Gas Source

The gas used in the HHG comes from the in-house supply of compressed air at NIST that has a pressure head of 550 kPa. Before entering the generator, the gas passes through a large regenerating gas dryer and CO_2 scrubber; this reduces the water mole fraction to 1×10^{-6} and removes 95 % of the CO_2. The CO_2 removal prevents a reaction between it and the saturator water that forms carbonic acid. After purification, the gas passes through a 240 L ballast tank which serves to minimize pressure pulses produced by the gas dryer. Computer-controlled mass flow controllers regulate the gas flow out from the tank; the maximum gas flow is 150 L/min.

4.2. Saturation System

The saturation system of the HHG consists of a pre-saturator and final saturator with a heatable tube connecting them. These parts are described below.

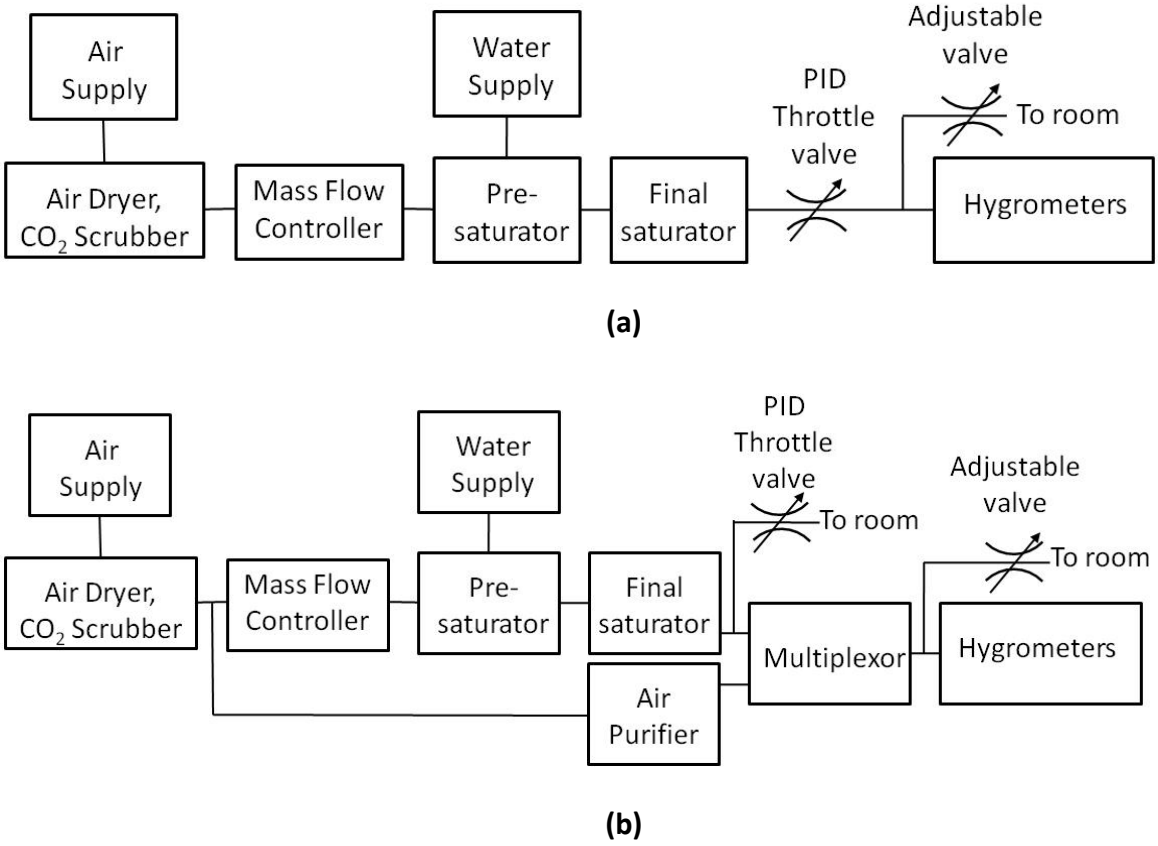

Figure 1. Schematic representation of the hybrid humidity generator (HHG) in a) two-pressure mode and b) divided-flow mode

4.2.1. Pre-saturator

The pre-saturator accomplishes virtually all of the saturation, and the final saturator performs small adjustments to ensure that the generated humidity is constant and determinable with minimal uncertainty.

The purpose of the pre-saturator is to allow the HHG to generate high water mole fractions with low uncertainty. For a thermodynamic generator to accomplish this, the dry carrier gas must be humidified to a dew-point temperature nearly equal to the final saturator temperature before entering the saturator. Since water vapor mole fractions in the HHG approach 0.57, operation without a pre-saturator would cause excessive latent heat loading on the final saturation process. This would introduce large temperature gradients in the final saturator, resulting in large uncertainties in the mole fraction of water in the gas.

A schematic diagram of the pre-saturator is shown in Fig. 2. It is a commercially made system that saturates the incoming gas by first passing the gas through its saturation chamber. In this chamber the gas is sprayed with water heated to about 10 °C above the desired saturation dew-

point. Afterwards the gas passes through the pre-saturator's heat exchanger, which is controlled at approximately the desired dew-point temperature. The gas's excess moisture condenses inside this heat exchanger and flows down to the pre-saturator's water reservoir.

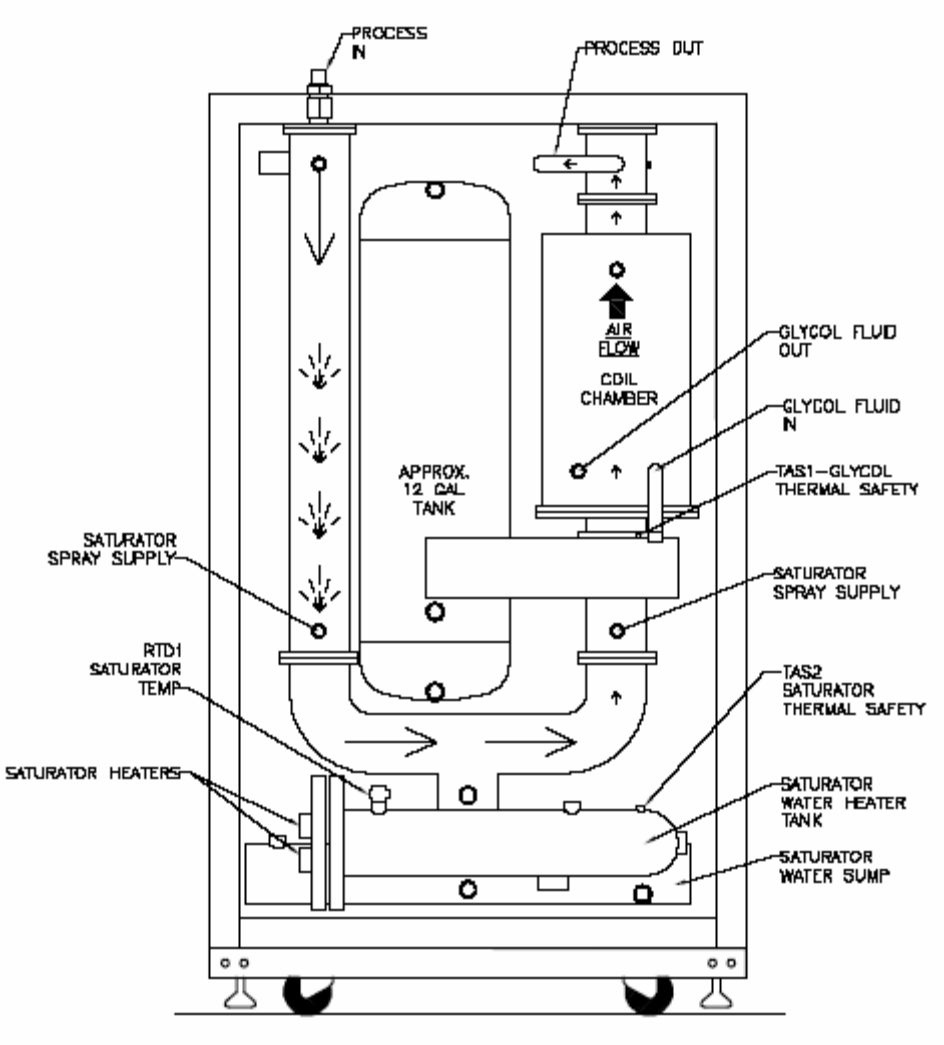

Figure 2. Schematic diagram of the pre-saturator of the HHG.

4.2.2. Connecting tube

The pre-saturator and final saturator are connected using 2.5 cm diameter stainless steel tubing. When dew points higher than the ambient temperature are to be generated, the tubing is temperature-controlled to be about 10 °C higher than the desired dew point in order to prevent water condensation in the tubing. To ensure a uniform temperature of the inner tube, with no cold spots where water could condense, the connecting tube is surrounded by an outer aluminum "shell" tube of inner diameter 7.3 cm and outer diameter 7.6 cm. Resistance heaters wound around this shell tube heat the shell tube to the desired temperature. Industrial process controllers with thermocouple sensors control the temperature of the shell tube. Heating of the

connecting tube is accomplished by heat transfer through air from the outer tube. Heating the connecting tube in this way generates less temperature non-uniformities on the tube than if the resistance heaters were directly attached to the tube.

4.2.3. Final Saturator

The final saturator is composed of a heat exchanger and saturation chamber. Both systems rest inside a commercially-made temperature-controlled bath of volume 167 L that is uniform to within 0.003 °C at 25 °C. The heat exchanger is located immediately above the saturation chamber in the bath. The gas first enters the heat exchanger, which conditions the gas to be at the temperature of the saturation chamber; this minimizes sensible heat loading on the chamber and also minimizes latent heat loading on it if the entering gas is oversaturated. In addition, the heat exchanger condenses out any moisture above the dew-point of the saturation chamber; this condensed water is then directed down into the saturation chamber. The heat exchanger is made of 316L stainless steel and is composed of two header tanks separated by an array of 116 parallel tubes with inner diameter 7.8 mm and length 48.5 cm. The parallel tube design minimizes the pressure drop across the heat exchanger. The diameter of the tubes is sufficiently large to prevent them from being blocked by condensed water droplets. With the tube dimensions described and with a gas flow of 150 L/min, the gas flows through the parallel tubes for a period of about ten thermal time constants.

The gas exiting the heat exchanger flows into the saturation chamber below. The chamber is flat and roughly rectangular in shape. The saturation chamber is also made of 316L stainless steel and contains a 2.2-cm layer of water and a 2.2 cm layer of gas above it. The chamber has a horizontal area of 0.28 m^2, with total water and gas volumes of 6.16 L each. Stainless steel dividers inside the saturator partition the chamber into two channels of width 3.7 cm that follow a serpentine path, as shown in Fig. 3. Each channel covers half the area of the saturation chamber, as shown. The dividers are continuously welded along their lengths into the top plate of the chamber, allowing no gas flow over the dividers. Twisted vanes are welded to the dividers to improve mixing between the gas and water vapor while the gas is in the saturation chamber.

Inside the saturation chamber, a rectangular cross section rather than a circular cross-section is used because the former exhibits less sensitivity to water height changes than would a circular cross-section design. For a given water level, the rectangular section contains more water volume and has a smaller rate of change in airway cross-sectional area with water level, relative to a circular cross section. Therefore, increases in water volume in the chamber (from water condensation in the heat exchanger) are less likely to restrict the airway; this allows the generator to produce very high dew-point temperatures for significant time periods.

After the final saturator was constructed, the stainless steel inside of it was commercially passivated to insure that the saturator would not contaminate the water stored in it. Since then, samples of water kept in the saturator for several months have been analyzed and show no noticeable increase in the level of impurities.

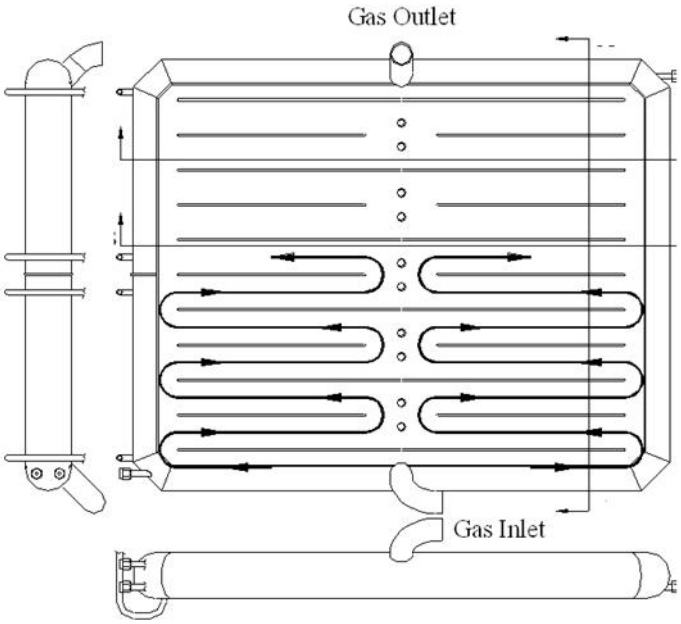

Figure 3. Schematic diagram of the saturation chamber.

The temperature of the final saturator is determined using a standard platinum resistance thermometer (SPRT) immersed in the temperature-controlled bath. The SPRT has been calibrated on the International Temperature Scale of 1990 (ITS-90) by the NIST Thermometry Group. The resistance of the SPRT is measured using a computer-interfaced AC resistance bridge with a temperature-controlled 25 Ω standard resistor as the reference resistor. A pressure transducer based on a silicon strain gauge, interfaced to a computer, measures the pressure in the saturator; the gauge is connected to a point in the saturator near the gas outlet using ¼ inch (0.635 cm) stainless-steel tubing. This tubing is at a sharp vertical slope in the region immediately above the saturator. Therefore, when the saturator is above the ambient temperature, any condensation occurring in the tubing is directed down to the saturator; this ensures that the transducer is never exposed to condensed water and always properly measures the pressure inside the saturator. Chamber pressure measurements (for dew point determination) are also made with a pressure transducer based on a silicon strain gauge. Both transducers have been calibrated against a piston gauge that has been calibrated by the NIST Pressure and Vacuum Group.

The entire heat-exchanger/final-saturator system is shown in Fig. 4. A horizontal plate on top of the heat exchanger supports the system inside the temperature-controlled bath and also serves as the top cover to the bath. Two sets of water fill tubes and exit tubes can be seen in the figure, one for each channel. The fill tubes are used to fill the saturation chamber with water. The exit tubes are used to withdraw water that is above the fill level; this is accomplished by applying a vacuum to the tubes. When viewed from above, the saturator and heat exchanger nearly fill the bath chamber, and almost touch a baffle plate attached to the two bath stirrers (see figure). This configuration promotes optimal circulation of water within the bath, with minimal dead-zones. Such a design minimizes temperature-non-uniformity in the bath.

4.3. Implementation of the Two-Pressure Method

The two pressure technique [6] involves saturating the gas at an elevated pressure and afterwards expanding the gas down to ambient pressure. The advantage of this technique is that a range of humidity values can be generated using one saturator temperature. This is useful for two reasons. First, it is much faster for an operator to change the saturator pressure than to change the saturator temperature. Secondly, the low humidity limit of the generator is lowered, since the molar fraction is inversely proportional to the saturator pressure.

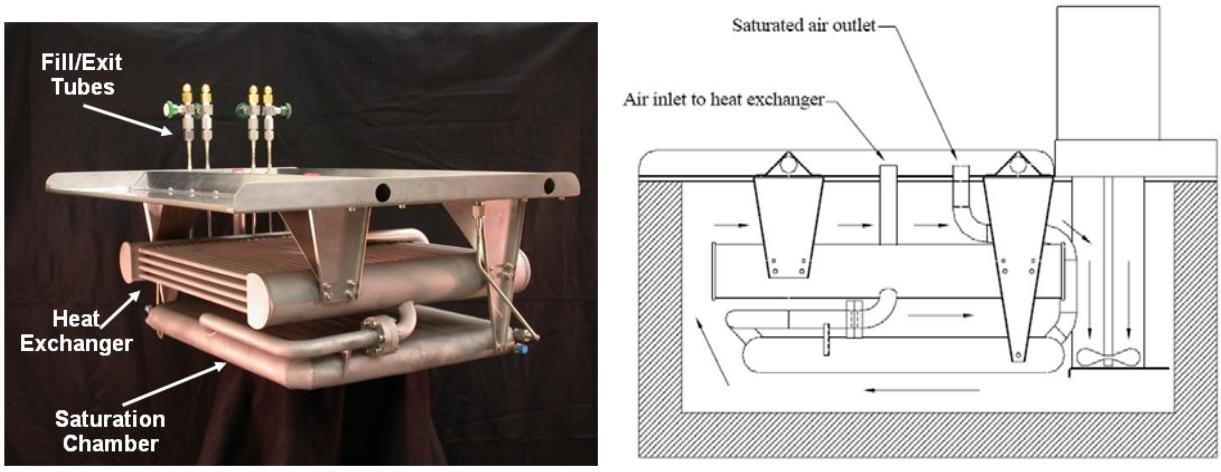

Figure 4. The final saturator. Photograph of the saturator, showing the heat exchanger and saturation chamber (left), and schematic diagram of the saturator in the temperature-controlled bath, showing direction of water flow in the bath (right).

The HHG employs the two-pressure technique by first using the 550 kPa pressure head of the gas source to raise the pressure in the saturator. It then uses an expansion valve at the exit of the saturation chamber to control the pressure. The expansion valve consists of a throttle valve with a high-speed motor/gear assembly. A PID controller that senses the pressure using the strain gauge mentioned above sets the opening of the throttle. The valve is located immediately above the temperature-controlled bath and is connected to the gas outlet from the saturator. Figure 5 shows a photograph of the laboratory layout of the pre-saturator, saturator, connector tube, and throttle valve.

4.4. Implementation of the Divided-Flow Method

The divided-flow method [6] involves diluting the saturated gas with dry gas using precisely-metered streams of gas. The mole fraction after dilution is

$$x = \frac{\dot{n}_s x_s + \dot{n}_p x_p}{\dot{N}} \qquad 6)$$

where $\dot{n}_s$ and $\dot{n}_p$ are the molar flows of the saturated gas and pure gas, respectively, and $\dot{N}$ is the total molar flow. Also, x_s is the molar fraction of water in the saturated gas and x_p is the residual molar fraction of water in the pure gas; the value of x_p is determined both from the efficiency of the gas purifier and from water outgassing from the tube walls of the manifold. Such a technique allows generation of arbitrarily low humidity values while operating the saturator at convenient temperatures. When generating low humidity, this method has two principal advantages. First, the temperature-controlled bath may be operated with water, which is much safer and less expensive than liquids with lower freezing temperatures. Secondly, the technique avoids the large temperature gradients in the generator bath that often exist at low temperatures; these gradients add large uncertainties to the uncertainty of the generated humidity.

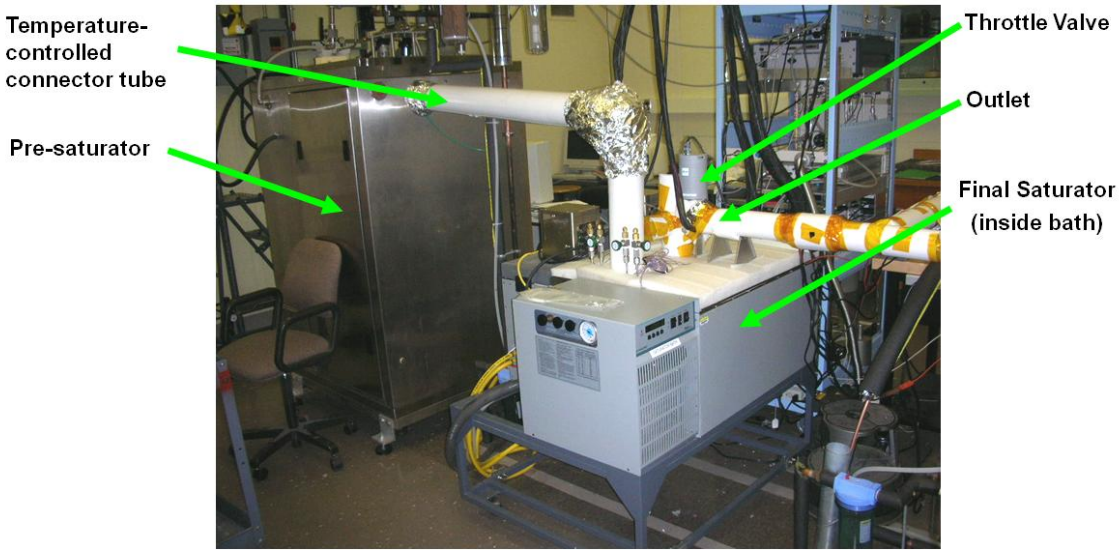

Figure 5. Laboratory configuration of several components of the HHG.

The HHG employs the divided-flow method using a gas multiplexer. The multiplexer contains seven flow-metering banks. Each bank consists of a commercially-made mass-flow controller and a commercially-made flow meter (a laminar-flow element) that measures the standard volume flow. The metering ranges of the flow meters are 10 cm^3/min, 100 cm^3/min, 1 L/min, 10 L/min, 30 L/min, 100 L/min, and 100 L/min. The upstream side of each flow bank is connected in parallel to both the saturated gas supply and a purified gas supply. When the divided flow method is used, both the saturated gas supply (and hence the saturator) and the purified gas are kept at a pressure of approximately 300 kPa. The purified gas comes from the original gas source described in section 2.1, but it is additionally dried using a molecular sieve; the sieve is specified to reduce the water mole fraction of the gas to 1×10^{-9}. The downstream side of each flow bank connects to a common outlet manifold. Pneumatic valves controlled by a computer select whether dry gas, wet gas, or no gas flows through each bank. For those banks with flow, the computer-controlled mass-flow controllers adjust the flow to provide the dilution nominally specified. The flow meters measure the flow of the saturated gas $\dot{\upsilon}_s$ and the flow of the dry gas $\dot{\upsilon}_p$ and provide this information to the computer. The two flows are added to obtain the total

flow $\dot{V}$. The flow meters have been calibrated for pure air by the NIST Fluid Metrology Group, using upstream pressures of 300 kPa to replicate the conditions under which they are used. When measuring the air flow of the saturated gas (with $x = 0.0022$), it is assumed that the change to the flow-meter calibration due to the saturation is negligible. It is also assumed that $\dot{n}_s / \dot{N} = \dot{\upsilon}_s / \dot{V}$ and $\dot{n}_p / \dot{N} = \dot{\upsilon}_p / \dot{V}$. Combining the above assumptions has been shown to cause an error of less than $3.5 \times 10^{-4} \dot{n}_s$, which is below the calibration uncertainties for the flow meters. Figure 6 shows a photograph of the multiplexer.

5. Performance and Validation Tests

Performance tests were made on the HHG in two-pressure mode to determine components of an uncertainty budget for the generator. Specifically, we measured temperature gradients and temperature stability in the saturator bath, and temperature gradients and pressure stability inside the saturation chamber.

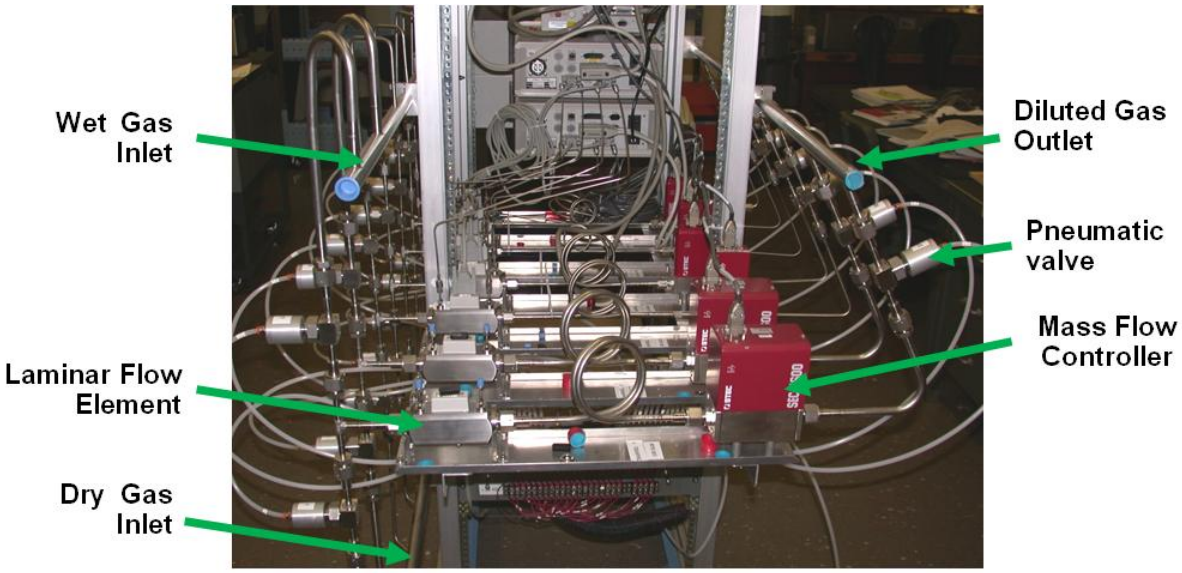

Figure 6. Photograph of the multiplexer, which is used when operating the HHG in divided-flow mode.

5.1. Temperature Uniformity and Stability in Final Saturator

We measured temperature non-uniformities in the bath with five type K thermocouples used in differential mode, measured with an 8 ½ digit multimeter through a scanner with low thermal emfs. We attached the reference junction of each thermocouple to the exit point from the saturator chamber, and placed the measuring junction in thermal contact with the location of

interest. The locations examined were the entrance to the heat exchanger, the exit from the heat exchanger, the entrance to the saturation chamber, the bath below the saturation chamber, and the bath above the saturation chamber.

Figure 7 shows the temperature non-uniformities measured. In a) they are shown as a function of bath temperature with no gas flow. Between 0 °C and 40 °C, the non-uniformities are within the resolution of the measurements. At 60 °C non-uniformities become observable and at 85 °C they reach 16 mK. However, the largest non-uniformities are vertical, with the top of the bath being cooler than the bottom, and it has been found that the largest temperature variation (at the top of the bath by the entrance to the heat-exchanger) is strongly dependent on the bath fill level. In b) they are shown at 84 °C as a function of gas flow when the pre-saturator temperature is 85 °C. Here, the non-uniformities are plotted as a function of time; before 1800 s the flow is zero, and after 1800 s the flow is 150 L/min. No significant difference in the non-uniformities is seen for these two flows. Note that the non-uniformity at the entrance to the heat exchanger is noticeably smaller in b) than in a); we attribute this to a higher bath fill level in b). In b), the non-uniformity in the bath above the heat exchanger is not shown because the corresponding thermocouple was not functioning when the measurements were made. As a result of these studies, we have concluded that during humidity calibrations the fill level of the bath should always be approximately 2.5 cm below the top lid of the bath container.

We also measured the thermal effects of pre-saturated gas flowing through the saturator. The measurements were made using two metal-sheathed, type T thermocouples that are mounted with measuring junctions near the saturator entrance. The junction of the first thermocouple is immersed in the water and that of the second is located in the gas stream. Figure 8 shows the temperature difference between the thermocouple junctions when gas flows through the generator and when no gas flows through (with no flow, we assume both thermocouples are at the bath temperature). For this plot, the bath temperature is 22 °C, the gas flow is 50 L/min and the differences are plotted as a function of pre-saturator dew point. When the pre-saturator dew point is considerably less than the bath temperature, temperature non-uniformities occur due to evaporative cooling of the water in the chamber. With a dew-point 8 °C below the bath temperature, the non-uniformity is over 0.1 °C. However, no non-uniformities are resolvable when the dew point is above the bath temperature; in this case the excess moisture condenses in the heat exchanger and the gas is at thermal equilibrium with the saturation chamber by the time it enters the chamber. These measurements demonstrate the importance of setting the pre-saturator to a dew point above rather than below the bath temperature.

In addition, we measured the stability of the bath over 1200 s at a series of bath temperatures. Figure 9 shows the results. At 20 °C the standard deviation was at a minimum, at 0.2 mK. As the bath temperature was lowered, the standard deviation reached 0.9 mK at 0.5 °C and, as it was raised, the standard deviation reached 1.1 mK at 85 °C.

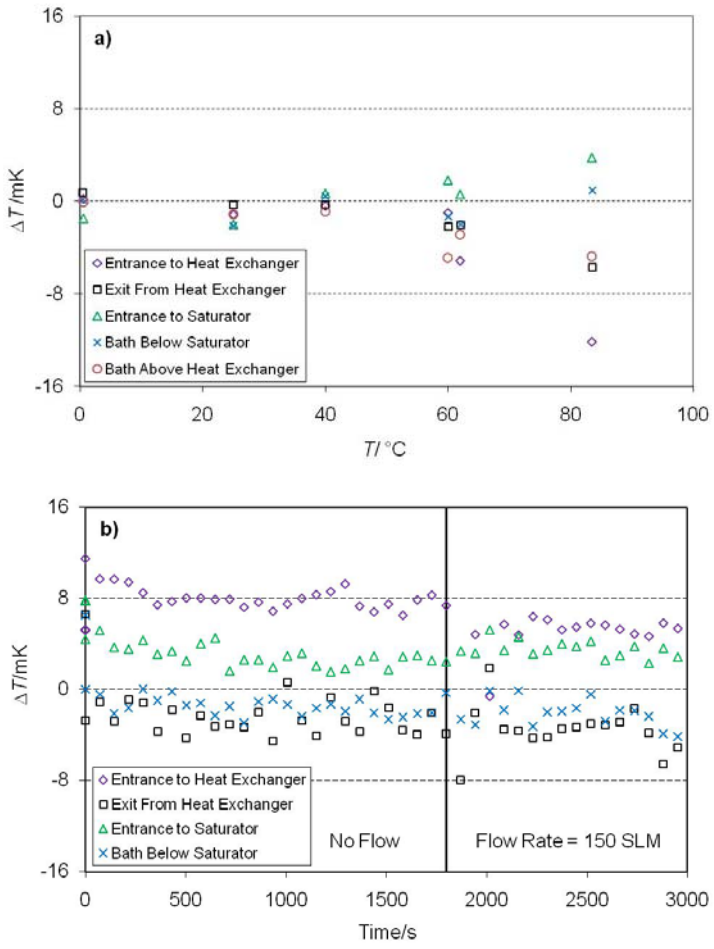

Figure 7. Temperature non-uniformities in the bath containing the final saturator, as measured by differential type K thermocouples attached to the outside of the saturator. The plots display temperature differences between the designated location and the exit point from the saturation chamber. In a), the non-uniformities are shown as a function of bath temperature when no gas flows through the generator. In b), the effect of gas flow on the non-uniformities is shown for a temperature of 84 °C. The non-uniformities are shown as a function of time, with no flow before 1800 s and 150 L/min after 1800 s. Here, the saturator is at ambient pressure and the pre-saturator is generating a dew point of 85 °C).

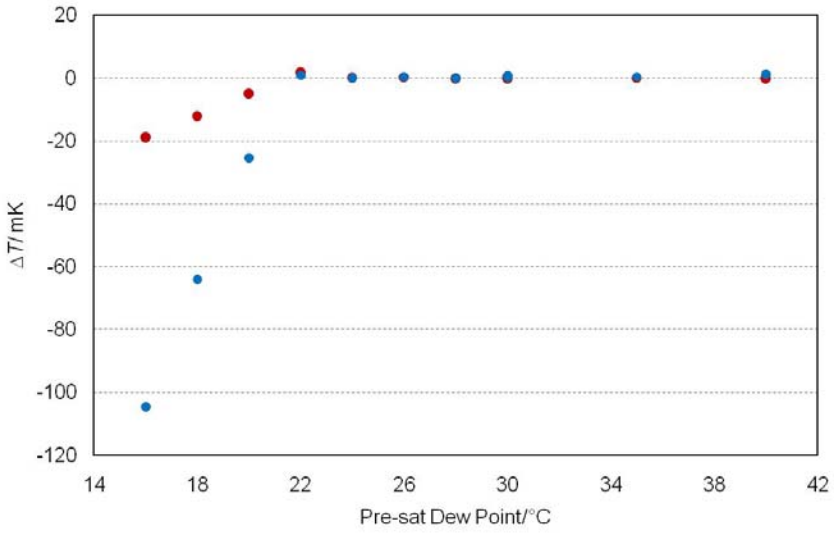

Figure 8. Temperature deviations from the bath temperature inside the saturation chamber at the entrance to the chamber when gas is flowing through it. The flow is 50 L/min and the bath temperature is 22 °C. The deviations are plotted as a function of pre-saturator dew point. The blue and red circles are from type T thermocouples (used in absolute mode) placed in the water and gas, respectively. Here, $\Delta T = T_{\text{flow}} - T_{\text{no flow}}$, where T_{flow} and $T_{\text{no flow}}$ are the measured temperatures with and without gas flow, respectively. $T_{\text{no flow}}$ is assumed to be the bath temperature.

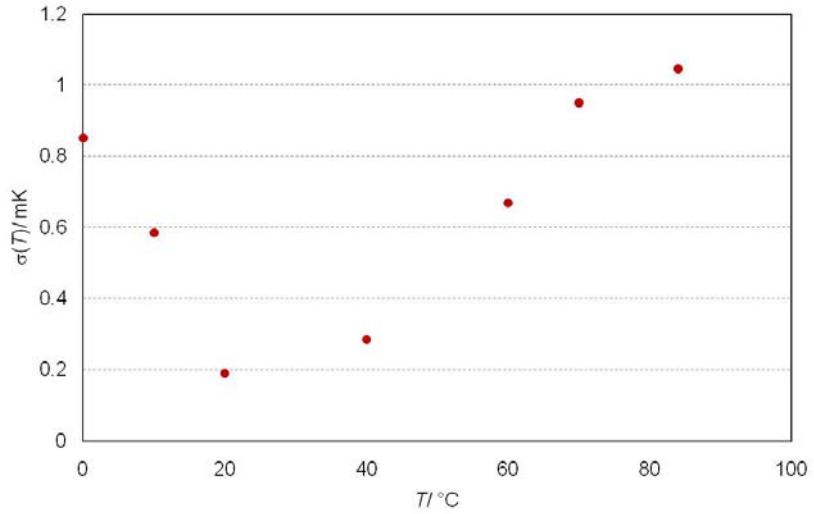

Figure 9. Standard deviation of the temperature fluctuations in the bath containing the final saturator as a function of bath temperature, as measured by an SPRT.

5.2. Pressure Stability in the Final Saturator

For measuring pressure fluctuations in the saturation chamber, we first optimized the PID settings of the pressure controller. We then measured the pressure variations at the optimum settings. At a saturator temperature of 20 °C and with a variety of pressures and flows up to 150 L/min, the standard deviation was less than 15 Pa. An example is shown in Fig. 10, where the flow was 100 L/min, and the standard deviation of the pressure fluctuations was 9 Pa. Unfortunately, since pressure is controlled by adjustments of gas flow out of the saturation chamber, optimal pressure control results in noticeable gas-flow fluctuations. Gas flow fluctuations can cause mirror-temperature instabilities for chilled-mirror hygrometers, preventing them from achieving optimal resolution. Therefore, less-than-optimal PID settings may be required to keep gas-flow fluctuations at acceptable levels. The level of fluctuations that is acceptable must be determined for each hygrometer.

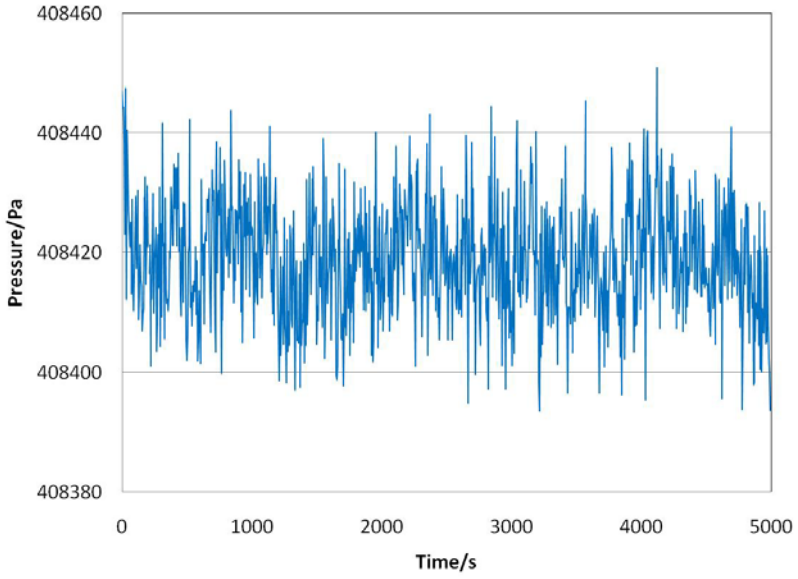

Figure 10. Pressure fluctuations in the saturator when the flow is 150 L/min. The standard deviation of the fluctuations is 9 Pa.

5.3. Self-consistency of the Generator in 2-P Mode

For the self-consistency tests, we generated dew points with eight different saturator temperatures and saturator pressures ranging from 500 kPa to ambient. By varying the degree of pressure expansion, the same dew point may be generated over a range of saturator temperatures. Self-consistency of the generator output was tested by using a chilled-mirror hygrometer as a transfer standard. We performed a 4-wire resistance measurement of the hygrometer's platinum resistance thermometer (PRT), which is in thermal contact with its mirror. The hygrometer dew-point temperature, as determined by the PRT, was then calculated with the Callendar-van Dusen equation [11], using 100 Ω as the assumed PRT resistance at 0 °C. The flow through the

generator was 30 L/min, and 0.5 L/min of this flow was directed through the hygrometer. The difference between the hygrometer-measured dew point temperature and the generated dew point temperature, ΔT_{DP}, was then plotted for each dew point of the set. Figure 11 shows ΔT_{DP} as a function of dew point temperature. The overlap between the dew points generated at different saturator temperatures, indicated with different symbols, shows the degree of self-consistency of the HHG. The dew point values agree with each other to within 20 mK.

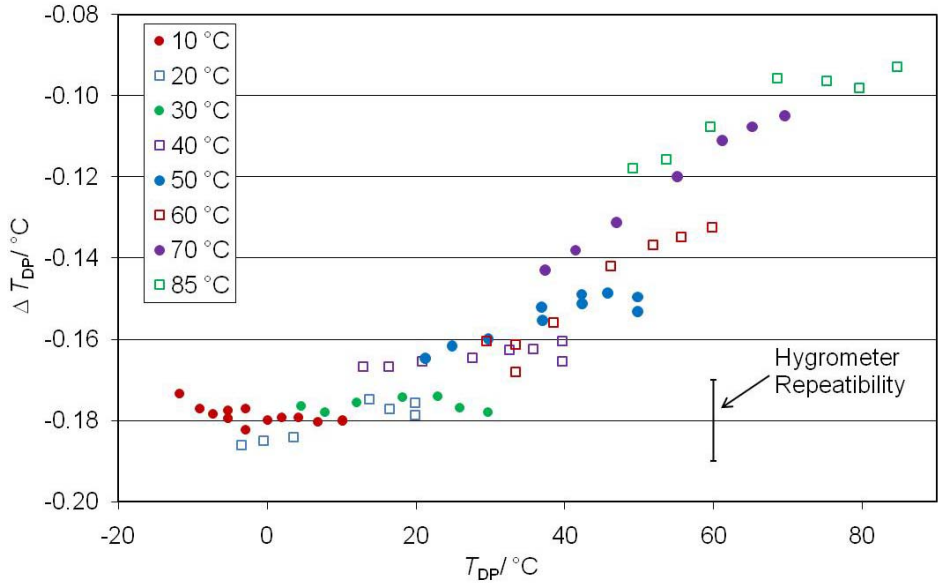

Figure 11. Comparison of dew points generated by the HHG using different saturator temperatures. The comparisons were made using an uncalibrated chilled-mirror hygrometer as a transfer standard. Here ΔT_{DP} is the measured dew point minus the generated dew point. Measurements with the saturator at different temperatures are plotted with different symbols. The hygrometer repeatability ($k = 1$) is shown as an error bar.

6. Uncertainty Budget

Based on these performance tests as well as measurement equipment specifications, we have constructed uncertainty budgets for the humidity generated by the HHG. There are budgets for the two expressions of humidity (mole fraction and dew/frost-point) under two conditions: two-pressure generator without dilution and two pressure with dilution. The total uncertainties associated with these budgets are based on the ISO and NIST guidelines for the expression of uncertainty in measurement [12,13]. The equations relating the total uncertainties to the uncertainty components are listed below and derived in Appendix I.

The total uncertainty for humidity generated by the hybrid generator is presented here for four different humidity definitions: water mole fraction, dew/frost-point temperature, relative humidity, and mass ratio. For each of these four definitions, we present the uncertainty for the cases of humidity generated in 1-P mode, 2-P mode, and divided-flow mode. In the equations below, $u(X)$ is the standard uncertainty of the quantity X.

6.1. Water Mole Fraction Generated in 1-P or 2-P Mode

Here, the total standard uncertainty for the water mole fraction, $u(x)$, is expressed as

$$u(x)^2 = \left(\frac{1}{P_s}\frac{de_s}{dT_s}\right)^2 u(T_s)^2 + \left(\frac{e_s}{P_s^2}\right)^2 u(P_s)^2 + \left(\frac{1}{P_s}\right)^2 u\left(e_s^{calc}\right)^2 + \left(\frac{e_s}{P_s}\right)^2 u\left(f_s^{calc}\right)^2 . \quad 7)$$

The four relevant uncertainties are $u(T_s)$, $u(P_s)$, $u\left(e_s^{calc}\right)$and $u\left(f_s^{calc}\right)$. Here, $u\left(e_s^{calc}\right)$and $u\left(f_s^{calc}\right)$ are the uncertainties of the calculated values of $e(T_s)$ and $f_s(T_s,P_s)$, respectively, due to the imperfect knowledge of these physical relations.

6.2. Dew-point Temperature Generated in 1-P or 2-P Mode

For this case, the total standard uncertainty of the dew-point temperature T_{DP} or frost-point temperature T_{FP} of the gas in a test chamber with pressure P_c and temperature $T_c = T_{DP}$ or $T_c = T_{FP}$ is expressed as

$$u(T_{DP})^2 = \left(\frac{e_c}{[de_c / dT_{DP}]}\right)^2 \left[\left(\frac{1}{e_s}\frac{de_s}{dT_s}\right)^2 u(T_s)^2 + \frac{u(P_s)^2}{P_s^2} + \frac{u(P_c)^2}{P_c^2} + u\left(\Delta f^{calc}\right)^2 + u\left(\Delta e_r^{calc}\right)^2\right] \quad 8)$$

The five relevant uncertainties are $u(T_s)$, $u(P_s)$, $u(P_c)$, $u\left(\Delta e^{calc}\right)$and $u\left(\Delta f^{calc}\right)$. When the generator is used in 1-P mode ($P_s \cong P_c$),

$$u\left(\Delta e_r^{calc}\right) = u\left(\Delta f^{calc}\right) = 0 . \quad 9)$$

When the generator is used in 2-P mode ($P_s \neq P_c$),

$$u\left(\Delta e_r^{calc}\right)^2 \equiv \frac{u\left(e_s^{calc}\right)^2}{e_s^2} + \frac{u\left(e_c^{calc}\right)^2}{e_c^2} , \quad 10)$$

$$u\left(\Delta f^{calc}\right)^2 \equiv u\left(f_s^{calc}\right)^2 + u\left(f_c^{calc}\right)^2 . \quad 11)$$

Here, $u\left(e_c^{calc}\right)$and $u\left(f_c^{calc}\right)$ are the uncertainties of the calculated values of $e(T_c)$ and $f_c(T_c,P_c)$, respectively, due to the imperfect knowledge of these physical relations. In Eq. 10, note that the subscript "r" in Δe_r^{calc} is used to show that it is a relative quantity and therefore dimensionless.

6.3. Relative Humidity Generated in 1-P or 2-P Mode

The total standard uncertainty for relative humidity, $u(RH)$, of the gas in the test chamber with temperature T_c and pressure P_c is expressed as

$$u(RH)^2 = \left[\frac{P_c e_s}{P_s e_c}\right]^2 \left[\left(\frac{1}{e_s}\frac{de_s}{dT_s}\right)^2 u(T_s)^2 + \frac{1}{P_s}u(P_s)^2 + \left(\frac{1}{e_c}\frac{de_c}{dT_c}\right)^2 u(T_c)^2 + \frac{1}{P_c}u(P_c)^2 + u\left(\Delta e^{\text{calc}}\right) + u\left(\Delta f^{\text{calc}}\right)\right] \quad (12)$$

The six relevant uncertainties are $u(T_s)$, $u(P_s)$, $u(T_c)$, $u(P_c)$, $u\left(\Delta e^{\text{calc}}\right)$ and $u\left(\Delta f^{\text{calc}}\right)$. Here, $u\left(\Delta e^{\text{calc}}\right)$ and $u\left(\Delta f^{\text{calc}}\right)$ are given by Eqs. 10−11.

6.4. Water Mole Fraction Generated in Divided-flow Mode

For this case, $u(x)$ is expressed as

$$u(x)^2 \cong x^2\left[\left(\frac{1}{e_s}\frac{de_s}{dT_s}\right)^2 u(T_s)^2 + \frac{u(P_s)^2}{P_s^{\,2}} + \frac{u\left(e_s^{\text{calc}}\right)^2}{e_s^{\,2}} + u\left(f_s^{\text{calc}}\right)^2 + \frac{u(\dot{n}_p)^2}{\dot{N}^2} + \left(\frac{x_s}{x}-1\right)^2\left(\frac{u(x_p)^2}{x_s^{\,2}} + \frac{u(\dot{n}_s)^2}{\dot{N}^2}\right)\right] \quad (13)$$

The seven relevant uncertainties are $u(T_s)$, $u(P_s)$, $u\left(e_s^{\text{calc}}\right)$, $u\left(f_s^{\text{calc}}\right)$, $u(x_p)$, $u(\dot{n}_s)$ and $u(\dot{n}_p)$.

6.5. Frost-point Temperature Generated in Divided-flow Mode

In the hybrid generator, the divided flow method will only be used for generating frost points. Here, the total standard uncertainty of the frost-point temperature T_{DP} of the gas in the test chamber is

$$u(T_{FP})^2 = \frac{(xP_c)^2}{\left[de_c/dT_c\right]^2}\left[\left(\frac{1}{e_s}\frac{de_s}{dT_s}\right)^2 u(T_s)^2 + \frac{u(P_s)^2}{P_s^{\,2}} + \left(\frac{x_s}{x}-1\right)^2\left(\frac{u(x_p)^2}{x_s^{\,2}} + \frac{u(\dot{n}_s)^2}{\dot{N}^2}\right) + \frac{u(\dot{n}_p)^2}{\dot{N}^2} + \frac{u(P_c)^2}{P_c^{\,2}} + \frac{u\left(e_s^{\text{calc}}\right)^2}{e_s^{\,2}} + \frac{u\left(e_c^{\text{calc}}\right)^2}{(xP_c)^2} + u\left(\Delta f^{\text{calc}}\right)^2\right] \quad (14)$$

The nine relevant uncertainty elements are $u(T_s)$, $u(P_s)$, $u(x_p)$, $u(\dot{n}_s)$, $u(\dot{n}_p)$, $u(P_c)$, $u\left(e_s^{\text{calc}}\right)$, $u\left(e_c^{\text{calc}}\right)$ and $u\left(\Delta f^{\text{calc}}\right)$. Here, $u\left(\Delta f^{\text{calc}}\right)$ is defined in Eq. 11.

6.6. Relative Humidity Generated in Divided-flow Mode

Here, the total standard uncertainty of the relative humidity of the gas in the test chamber is

$$u(RH)^2 = \left[\frac{xP_c}{e_c}\right]^2 \left[\left(\frac{1}{e_s}\frac{de_s}{dT_s}\right)^2 u(T_s)^2 + \frac{u(P_s)^2}{P_s^{\,2}} + \frac{u\left(e_s^{\text{calc}}\right)^2}{e_s^{\,2}} + u\left(f_s^{\text{calc}}\right)^2 + \left(\frac{x_s}{x} - 1\right)^2 \left(\frac{u(x_p)^2}{x_s^{\,2}} + \frac{u(\dot{n}_s)^2}{\dot{N}^2} \right) + \frac{u(\dot{n}_p)^2}{\dot{N}^2} \right] + \left(\frac{P_c}{e_c}\right)^2 \left(x + \frac{\dot{n}_p}{\dot{N}} x_p \right)^2 \left[\frac{u(P_c)^2}{P_c^{\,2}} + \left(\frac{1}{e_c}\frac{de_c}{dT_c}\right)^2 u(T_c)^2 + \frac{u(e_c^{\text{calc}})^2}{e_c^{\,2}} + u(f_c^{\text{calc}})^2 \right] \quad (15)$$

The eleven relevant uncertainty elements are $u(T_s)$, $u(P_s)$, $u(x_p)$, $u(\dot{n}_s)$, $u(\dot{n}_p)$, $u(P_c)$, $u(T_c)$, $u\left(e_s^{\text{calc}}\right)$, $u\left(e_c^{\text{calc}}\right)$, $u\left(f_s^{\text{calc}}\right)$,and $u\left(f_c^{\text{calc}}\right)$.

6.7 Mass Ratio

The total standard uncertainty for mass ratio is related to that for the mole fraction by

$$u(r) = 0.6220 \frac{1}{(1-x)^2} u(x). \quad (16)$$

Here, $u(x)$ is given by Eq. 7 when the generator is used in 1-P or 2-P mode, and by Eq. 13 when the generator is used in divided-flow mode.

6.7. Uncertainty Elements

Shown in Table 1 is a list of all the relevant uncertainty elements mentioned above and their standard uncertainty values. The subcomponents of the uncertainty elements T_s, P_s, and P_c are given in Appendix II. The value for the uncertainty of T_c is based on the typical uncertainty for the calibration of external temperature probes at NIST. [14] The table does not contain all uncertainty elements for the calibration of hygrometers by the HHG, as the table does not include uncertainties from measurement repeatability of the particular hygrometer under calibration. In the calibration reports, however, the total uncertainty for the calibration of the hygrometer is reported, with the uncertainty due to hygrometer repeatability determined as described in section 8.4. In Table 1, the uncertainty for the calculation of $e(T)$ is obtained from Table 2 of [15]. The uncertainties for the calculations of f_s and f_c are presented as a fit to the uncertainty data of Table 9 in [16]; because there is no data below −50 °C, we extrapolated the curve determined from the available data to obtain the uncertainty formula listed in Table 1. In obtaining the formula, the "maximum percentage uncertainties" from [17] were divided by $\sqrt{3}$ to obtain the standard uncertainty. The values for $u\left(f_s^{\text{calc}}\right)$ and $u\left(f_c^{\text{calc}}\right)$ decrease with temperature and increase with pressure, and are quite significant for some operating conditions. By comparison, the uncertainties of e_s^{calc} and e_c^{calc} are negligible.

An additional uncertainty element is that due to moisture diffusion through the vertical pressure sensing tube of the final saturator. When the saturator temperature is above ambient, moisture will condense inside the tube in the ambient-temperature region and drip down to the saturator. As the air in that region dries from the condensation, additional moisture will diffuse through the tube from the saturator to the ambient-temperature region. This creates a diffusion-driven moisture flow which can lower the water mole fraction of the air exiting the saturator. We have calculated the depletion and determined it to be less than 0.002 % for the intended gas flows through the generator (over 20 L/min). This amount is negligible compared to other uncertainties, and as a result we are not including it in Table 1.

Table 1. Uncertainty elements for the Hybrid Humidity Generator and their uncertainties. Here, $u(X)$ is the standard uncertainty for element X. The elements with subscript "c" refer to the environment in which the humidity is to be determined. The element T_c is only relevant when the hygrometer uses an external thermometer for determination of relative humidity.

X	$u(X)$ $(k = 1)$	Condition	Unit
T_s	1.5	($T \leq 40$ °C)	mK
	$0.16T_s/°C - 4.9$	($T > 40$ °C)	
P_s	18	($P_s \approx$ ambient pressure)	Pa
	$\sqrt{29^2 + (P_s/10000\ \text{Pa})^2}$	($P_s >$ ambient pressure)	Pa
T_c	10		mK
P_c	15		Pa
e_s^{calc}	$44\times10^{-6}\, e_s^{calc}$		Pa
f_s^{calc}	$P_s/(10^7 \cdot \text{Pa})\ (18.3\ \text{K}/T_s - 0.047)$		--
e_c^{calc}	$44\times10^{-6}\, e_c^{calc}$		Pa
f_c^{calc}	$P_c/(10^7 \cdot \text{Pa})\ (18.3\ \text{K}/T_c - 0.047)$		--
x_p	10		nmol mol^{-1}
$\dot{n}_s$	$5\times10^{-4}\, \dot{n}_s$	($\dot{n}_s \geq 7.5\times10^{-6}$ mol s^{-1})	mol s^{-1}
	$1\times10^{-3}\, \dot{n}_s$	($\dot{n}_s < 7.5\times10^{-6}$ mol s^{-1})	mol s^{-1}
$\dot{n}_p$	$5\times10^{-4}\, \dot{n}_p$		mol s^{-1}

Figure 12 shows the total expanded uncertainty for humidity generated by the HHG when the generator is operated in 1-P mode. The uncertainty is shown for the a) mole fraction (relative uncertainty) and b) dew point. Here, the total expanded uncertainty is given by $U(x) = ku(x)$, where the coverage factor is $k = 2$. The expanded relative uncertainty is given by $U_r(x) = U(x)/x$. In the figure, the black curve represents the total uncertainty, while the other curves represent the contributions to the total uncertainty from individual uncertainty components. In Fig. 10(b), the uncertainty contributions from e_s^{calc} and e_c^{calc} are zero, because these uncertainties cancel out when the generator is used in 1-P mode; the uncertainty contributions for f_s^{calc} and f_c^{calc} are zero for the same reason. Also in this plot, the curve designated as "*P*" represents the contributions from both P_s and P_c. The figure shows that for the 1-P mode, the dominant uncertainty is from pressure measurement and stability, except for saturator temperatures above 60 °C; in this case uncertainties due to temperature non-uniformities in the bath dominate. Figures 13(a) and 13(b) show similar plots for the case when the generator is operated in 2-P mode with $P_s = 500$ kPa. In Fig. 13(b), the discontinuity at 0 °C is due to the assumption of frost-point generation below this temperature. This figure shows that when the saturator is operated in this way, the uncertainties in f_s^{calc} and f_c^{calc} usually dominate.

Figure 14 shows the expanded uncertainty generated by the HHG when it is used in divided-flow mode. The uncertainties plotted are (a) the water mole fraction (relative uncertainty) and (b) the frost-point temperature. For these plots, the saturator parameters are $P_s = 300$ kPa and $T_s = 0.5$ °C. In the plots, "*n*" refers to the combined contribution to the total from $\dot{n}_s$ and $\dot{n}_p$. In Fig 14(a), $U_r(x)$ is relatively constant for $x > 2\times10^{-5}$. At the highest value of x shown in the plot, $\dot{n}_p = 0$ and so $U_r(x)$ is only due to the saturator. As x decreases to 2×10^{-5}, $U_r(x)$ increases slightly due to the rising significance of $u(\dot{n}_s)$ and $u(\dot{n}_p)$. As x decreases below 2×10^{-5}, $u(x_p)/x$ dominates $U_r(x)$, increasing its value to nearly 1 % at $x = 2\times10^{-6}$. In (b), the total expanded uncertainty is $U(T_{FP}) = ku(T_{FP})$. For -55 °C $\le T_{FP} \le -12$ °C, $U(T_{FP}) \approx 14$ mK and is relatively constant over this entire range. As T_{FP} decreases below -55 °C, $U(T_{FP})$ rises rapidly up to 58 mK at -70 °C due to the increasing influence of $u(x_p)$.

Figure 15 shows the expanded relative uncertainty $U_r(RH) = U(RH)/RH$ for relative humidity calibrations using humid gas generated by the HHG and flowing to an environment with temperature $T_c = 20$ °C and pressure 100 kPa. Here, $U_r(RH)$ includes the uncertainty of the humidity produced by the generator and the uncertainty of the calibration of the hygrometer's external temperature probe. In plots a) and b) the generator is operated in 2-P mode; the plots show the uncertainty for two saturator temperatures: a) $T_s = 20$ °C and b) $T_s = 1$ °C, which generate different relative humidity ranges. In plot c) the generator is operated in divided-flow mode.

Figure 16 shows the total expanded relative uncertainty for mass ratio, $U_r(r) = U(r)/r$, generated by the HHG when the generator is operated in a) 1-P mode and b) 2-P mode with $P_s = 500$ kPa. In the plots, the black curve represents the total uncertainty, while the other curves represent the contributions to the total uncertainty from individual uncertainty components.

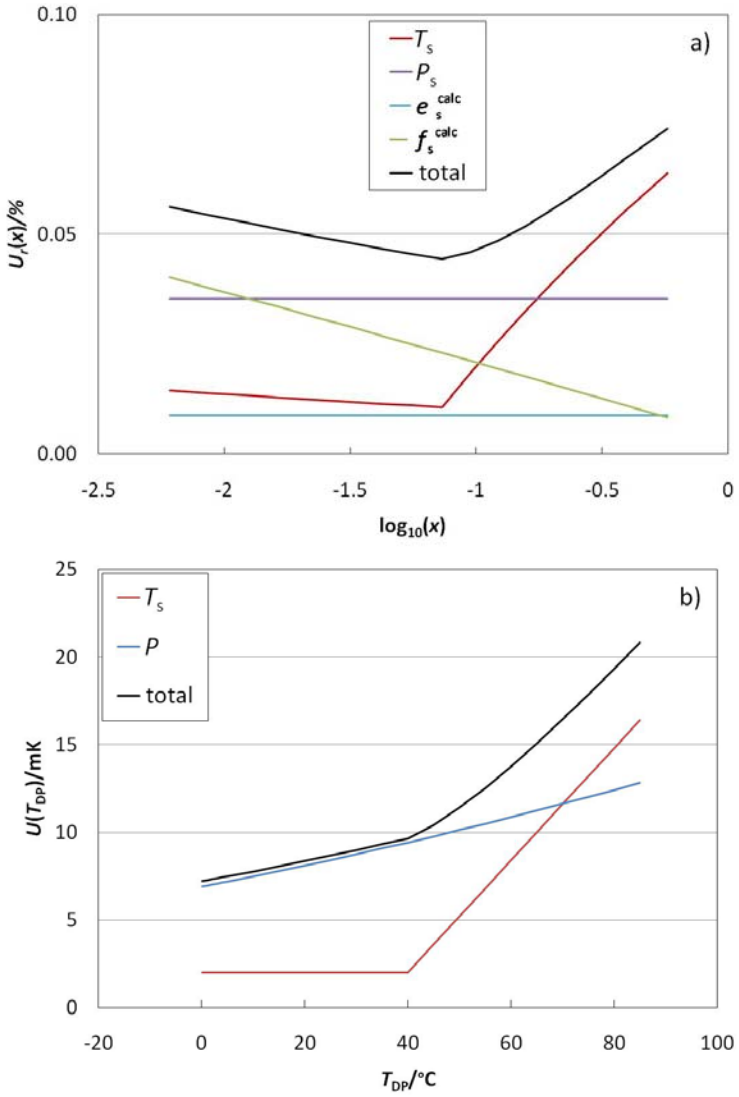

Figure 12. Total expanded uncertainty U for the (a) mole fraction and (b) dew-point temperature generated by the HHG saturator when used in 1-P mode. The black curve represents the total uncertainty, while the other curves show the contributions from individual uncertainty elements. In a), the expanded uncertainty is expressed as a relative uncertainty $U_r(x) = U(x)/x = ku(x)/x$, where $k = 2$ and $u(x)$ is the standard uncertainty for x. In b), the total expanded uncertainty is $U(T_{DP}) = ku(T_{DP})$. In b), P represents the combined contributions from both P_s and P_c.

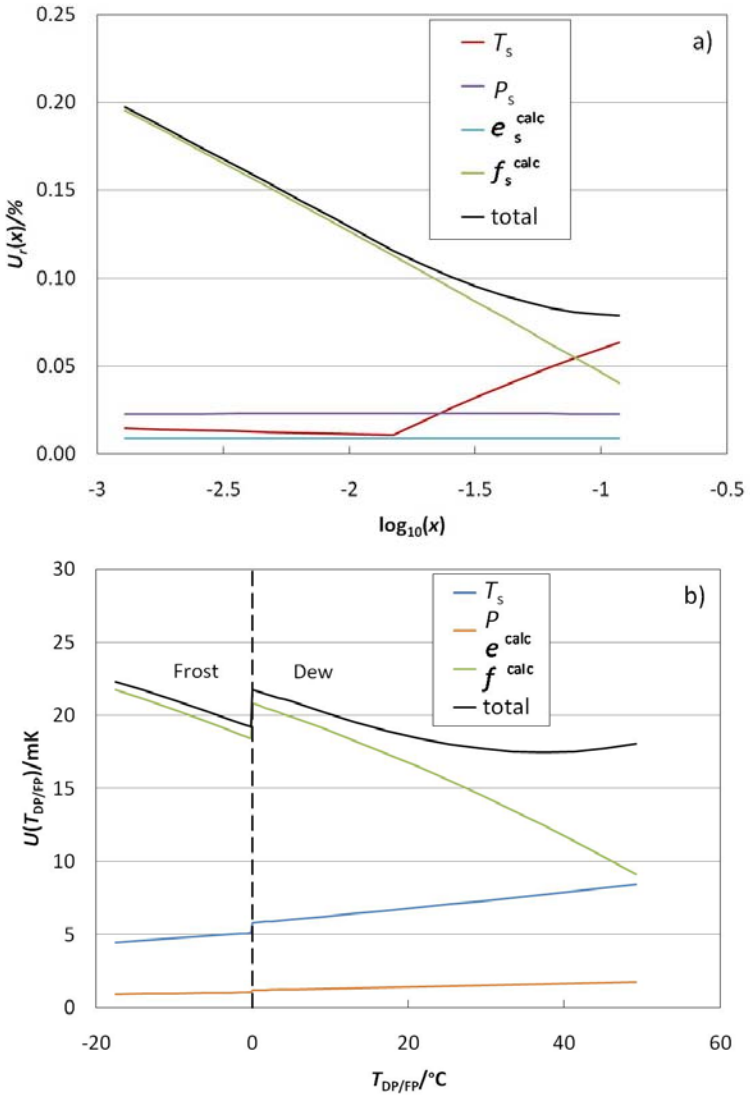

Figure 13. Total expanded uncertainty U for the (a) mole fraction and (b) dew/frost-point temperature generated by the HHG saturator when used in 2-P mode with P_s = 500 kPa. The black curve represents the total uncertainty, while the other curves show the contributions from individual uncertainty elements. In a), the expanded uncertainty is expressed as a relative uncertainty $U_r(x) = U(x)/x = ku(x)/x$, where $k = 2$ and $u(x)$ is the standard uncertainty for x. In b), the total expanded uncertainty is $U(T_{DP}) = ku(T_{DP})$. In b), P , e^{calc}, and f^{calc} each represent the combined contributions of their quantity from both the saturator and chamber (hygrometer).

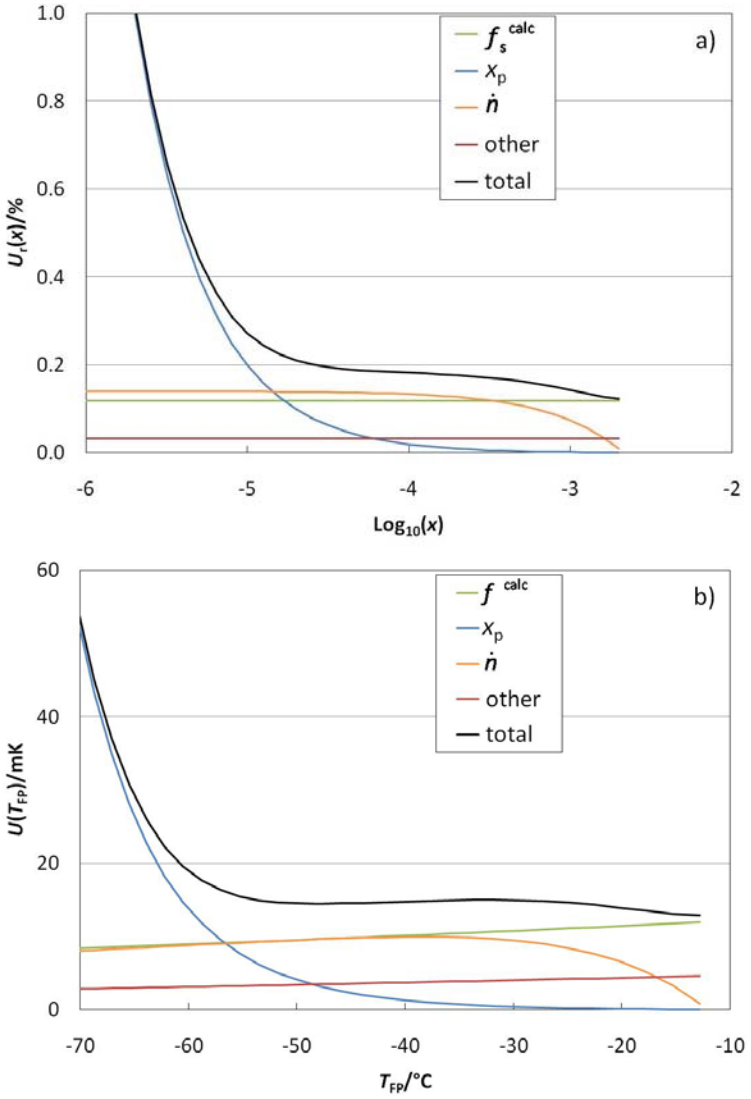

Figure 14. Total expanded uncertainty for the a) water mole fraction (relative uncertainty) and b) frost-point temperature generated by the HHG when it is used in divided flow mode with a saturator pressure of P_s = 300 kPa.). Here, f^{calc} represents the combined uncertainty contributions from both the saturator and chamber (hygrometer), and $\dot{n}$ represents the combined uncertainty contributions from the wet gas and dry gas.

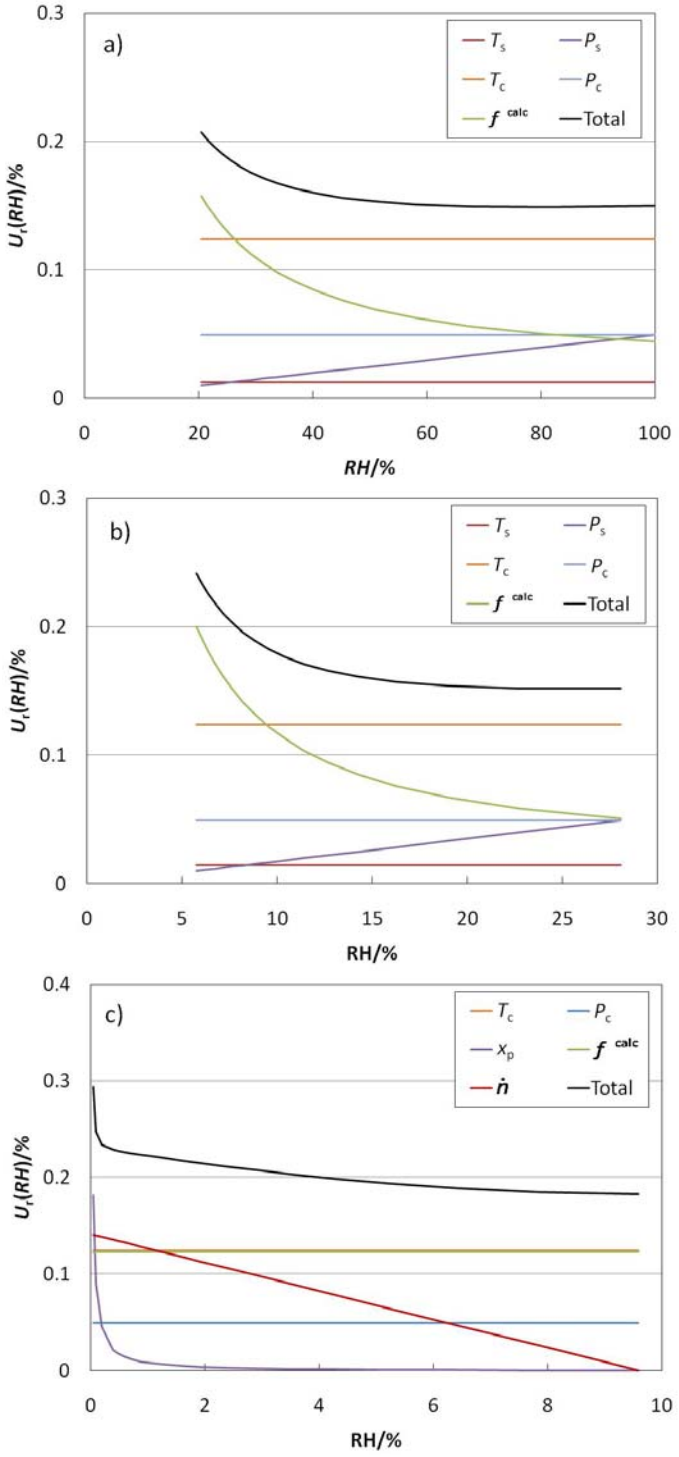

Figure 15. Total expanded relative uncertainty $U_r(RH)$ for the relative humidity calibrations using humid gas generated by the HHG to an environment of temperature T_c = 20 °C and pressure P_c = 100 kPa; here, $U_r(RH)$ includes the uncertainty for the calibration of the hygrometer's external temperature probe. In plots a) and b), the generator is used in 2-P mode, and the saturator temperature is a) 20 °C and b) 1 °C; the relative humidity is varied by changing the saturator pressure. In c) the generator is used in divided-flow mode.

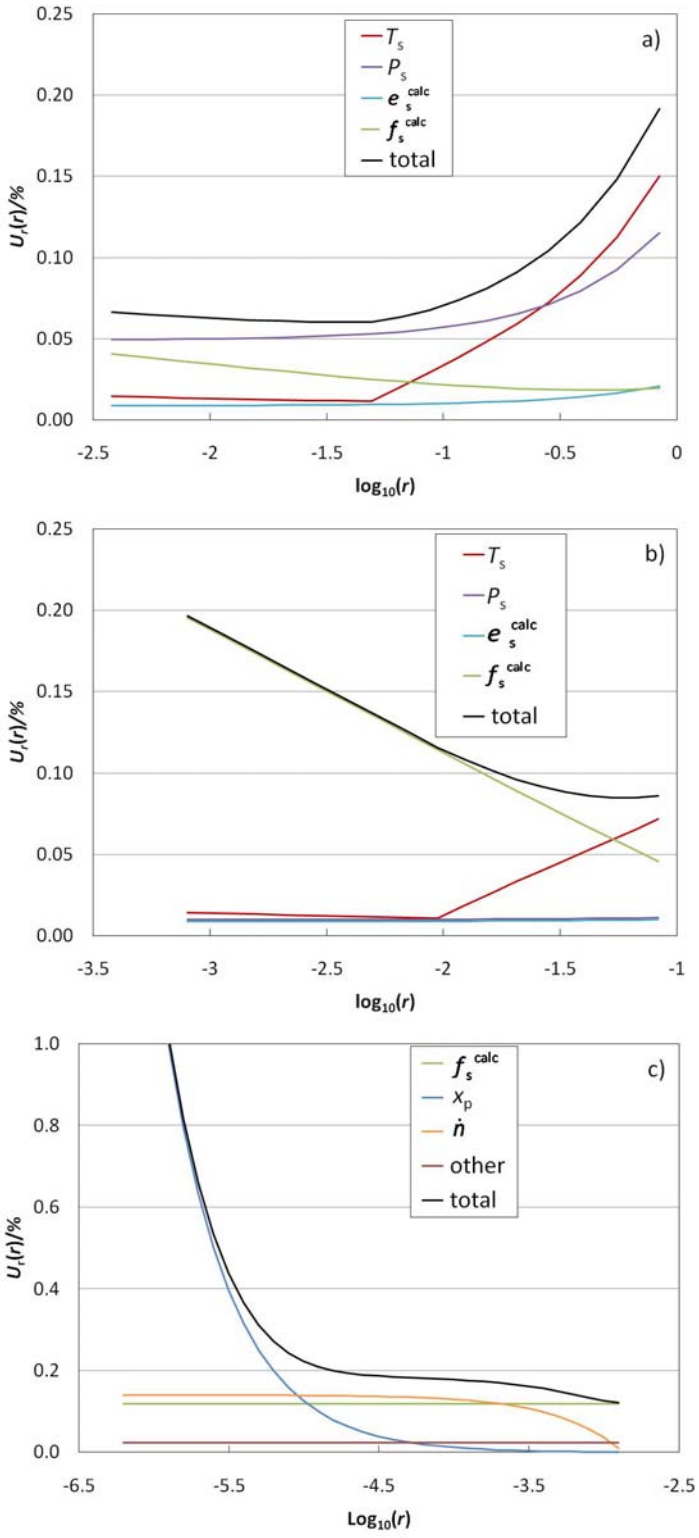

Figure 16. Total expanded relative uncertainty $U_r(r)$ for the mass ratio r generated by the HHG. In the plots the generator is used in a) 1-P mode, b) 2-P mode with P_s = 500 kPa, and c) in divided-flow mode.

7. Comparisons with other NIST Humidity Standards

7.1. Humidity Generators

To further validate the performance of the HHG and also determine the level of consistency between the NIST thermodynamic humidity generators, we made comparison measurements with the NIST 2-P generator Mark II [17] and the LFPG [18]. One set of comparisons was performed using the uncalibrated chilled-mirror hygrometer described in section 4 as a transfer standard. For the dew points generated, the expanded uncertainties (k=2) for the 2-P generator and LFPG are 40 mK [19] and 13 mK [18], respectively. In the LFPG, nitrogen was used as the gas source. Figure 17 shows the difference between the measured dew point and the expected dew point from the generator over the range −15 °C to 30 °C. The data from the HHG are those shown in Fig. 11. For measurements below 0 °C, the gas moisture was observed to condense on the mirror as dew rather than frost. The HHG and LFPG agree within 10 mK, which is within the combined expanded uncertainties of the two generators and the hygrometer. The HHG and 2-P generator agree within 40 mK; the difference is also within their combined expanded uncertainties, though only marginally so. We made a second set of comparison measurements against the LFPG over the frost point range −50 °C to −20 °C using a second chilled-mirror hygrometer. The comparison values and respective expanded uncertainties are shown in Figure 18. Once again, the HHG and LFPG agree within the combined expanded uncertainties of the two generators and the hygrometer over this range. Finally, a third set of comparison measurements was made against the LFPG over the low-humidity range. This time a commercial cavity ring down spectrometer served as the transfer standard hygrometer, which measured humidity in units of water mole fraction. The measurements were made over the range 1 μmol/mol to 5 μmol/mol (−76 °C to −65 °C frost point). To simplify the comparison, air was used as the gas source in the LFPG as well as in the HHG. The results, shown in Figure 19, agree to within the generators' expanded uncertainties. The results of these comparisons validate the performance of the HHG, showing that it generates correct humidity values to within its uncertainties.

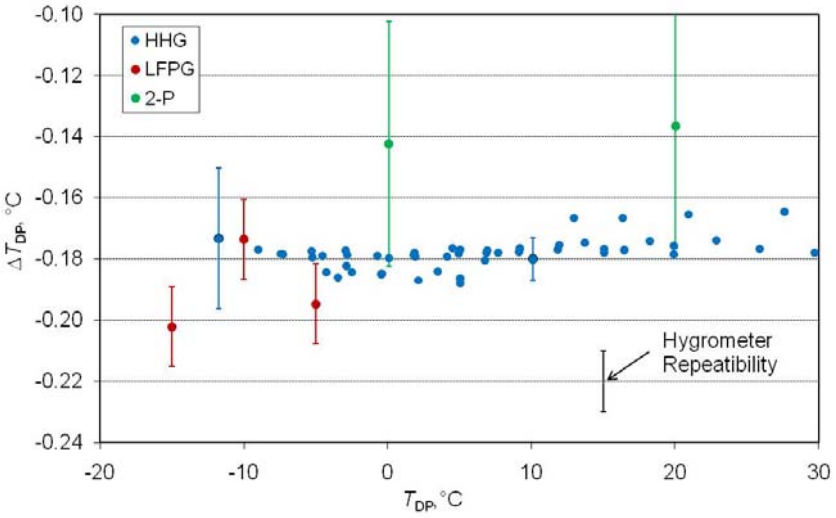

Figure 17. Comparison of dew points generated by the HHG with those generated by the NIST Two-pressure (2-P) generator and the NIST Low Frost-point Generator (LFPG). The comparisons were made using an uncalibrated chilled-mirror hygrometer as a transfer standard. Here, $\Delta T_{DP} = T_{DP\text{-}g} - T_{DP\text{-}h}$, where $T_{DP\text{-}g}$ is the dew point expected from the generator and $T_{DP\text{-}h}$ is the dew point measured by the hygrometer. The uncertainty bars reflect the expanded (k=2) uncertainties of the generators and hygrometer.

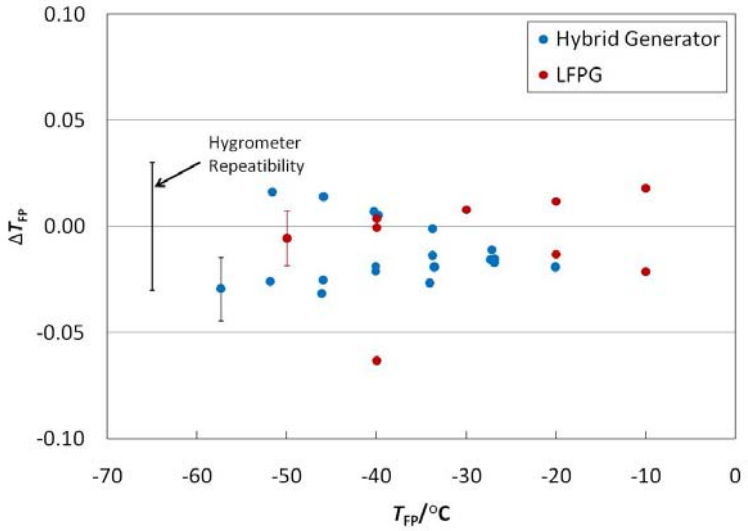

Figure 18. Comparison of frost points generated by the HHG with those generated by the LFPG. The comparisons were made using a second chilled-mirror hygrometer as a transfer standard. Here, $\Delta T_{FP} = T_{FP\text{-}g} - T_{FP\text{-}h}$, where $T_{FP\text{-}g}$ is the frost point expected from the generator and $T_{FP\text{-}h}$ is the frost point measured by the hygrometer.

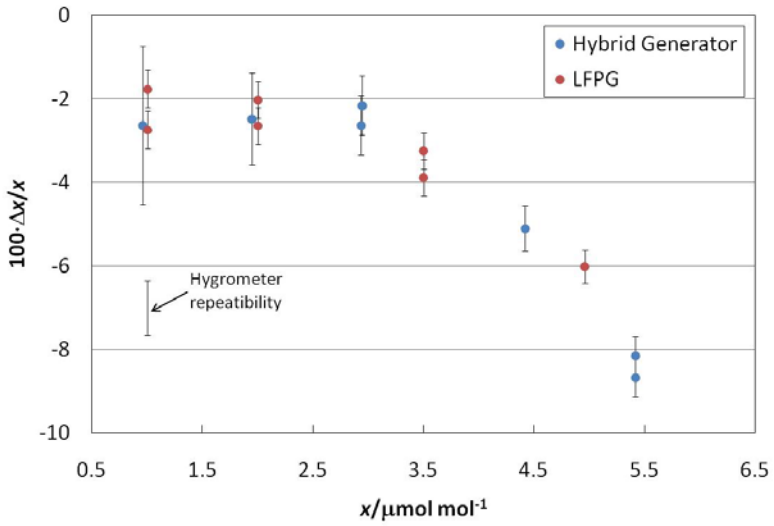

Figure 19. Comparison of mole fraction x generated by the HHG with that generated by the NIST Low Frost-point Generator. The comparisons were made using a commercial cavity ring down spectrometer as a humidity transfer standard. Here, $\Delta x = x_g - x_h$, where x_g is the mole fraction expected from the generator and x_h is the mole fraction measured by the hygrometer. The uncertainty bars reflect the expanded (k = 2) uncertainties of the generators.

7.2. Gravimetric Hygrometer

In addition to the comparisons reported in the previous section, we performed comparisons between the humidity generated by the HHG and that measured by the NIST gravimetric hygrometer [21,22]. The gravimetric hygrometer is a primary standard for humidity measurement. It determines the mass ratio of water to air in a humid gas sample by separating out the water from the gas and subsequently determining the masses of the water and dry air. The results of the comparison are shown in Figure 20, which plots $\Delta x/x$, where $\Delta x \equiv x_{GH} - x_{HHG}$; here, x_{GH} is the mole fraction measured by the gravimetric hygrometer and x_{HHG} is that generated using the HHG. Here, the saturator pressure was ≈200 kPa for all points except for those where $\log_{10}(x) = -2.7$. In this case the saturator pressure was 300 kPa and the saturator temperature was 1 °C; these are the saturator parameters used when the HHG is operated in divided-flow mode.

The expanded uncertainty (k = 2) of the mole fraction measurements by the gravimetric hygrometer is estimated to be 0.20 % over the range of humidity in the plot. For the hybrid generator using the above parameters, the expanded uncertainty is estimated to be less than 0.08 %, so the combined expanded relative uncertainty of the HHG and gravimetric hygrometer is estimated to be $U_r(x) \approx 0.22\%$.

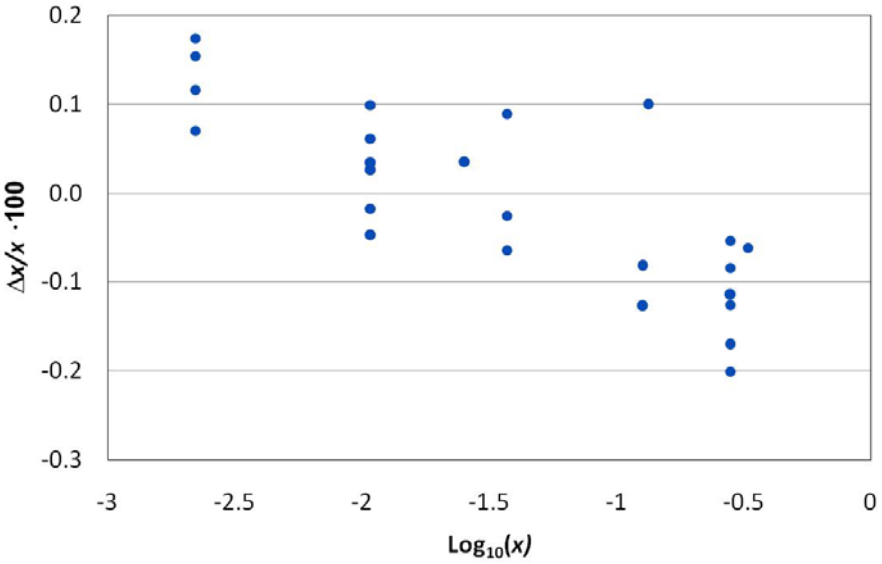

Figure 20. Comparison of mole fraction x measured by the NIST gravimetric hygrometer with that generated by the HHG. Here, $\Delta x \equiv x_{GH} - x_{HHG}$, where x_{GH} is the mole fraction measured by the gravimetric hygrometer and x_{HHG} is that generated using the HHG. The combined expanded (k = 2) relative uncertainties of the gravimetric hygrometer and generator are $U_r(x) \approx 0.22$ %.

The values of $\Delta x/x$ are all within 0.2 % and the averages of the points taken at one value of x are all within 0.12 %. This is within the combined uncertainties of the HHG and gravimetric hygrometer, showing agreement between the two systems.

8. Calibration of Hygrometers

8.1. General Method.

The calibrations are done at specific humidity points as requested by the customer. The hybrid generator temperature/pressure parameters are set to generate the desired humidity. For each nominal humidity point, a data-acquisition application is used to measure the temperature and pressure of the saturator, the pressure inside the hygrometers, and the wet-gas and dry-gas flows (if the divided flow method is used); these measurements are used to calculate the humidity inside the hygrometers. The application also records the humidity measurement of the customer hygrometer and check standard hygrometer. All measurements are recorded in a spreadsheet. Once the data is acquired for all requested humidity points, the results are assembled into a workbook. The new check standard data is compared to previous check standard data to validate the performance of the generator during this set of measurements. The final results comparing the customer hygrometer humidity to the HHG humidity are placed in a calibration report. For calibrations of chilled-mirror hygrometers measuring relative-humidity, dew-point calibrations are made using the generator, and subsequently a comparison calibration is made of the temperature probe in a stirred bath [14].

8.2. Initial Procedures.

Before connecting the hygrometers to the hybrid generator, they are checked for cleanliness; any noticeable dirt inside a hygrometer or on its fittings is grounds for rejecting the instrument for calibration. For the case of chilled-mirror hygrometers, we clean the hygrometer mirrors with ethanol. Finally, tests are performed to ensure that calibration points requested for each hygrometer are within its measurement range.

The pressure gauges of the hybrid generator are prepared for operation by correcting the zero offset for their readings. This is done by exposing the two gauges to a vacuum to measure their zero-offset values. The new values are entered into the data acquisition application to ensure accurate pressure measurements during the calibration.

8.3. Connecting the hygrometers to the hybrid generator.

When connecting the hygrometers to the generator, a bypass tube (with an outlet into the room) is connected in parallel with the hygrometers (see Fig. 21). A valve on the bypass tube allows control of the proportion of output gas bypassing the hygrometers. As seen in the figure, a gauge located between the hygrometers and the bypass valve measures the hygrometer pressure. In this configuration, no gas flowing into the hygrometers passes through the line for the gauge.

If the desired humidity values exceed a frost point of −15 °C ($x = 1.6 \times 10^{-3)}$, the hygrometers are connected directly to the output of the 2-P generator, at a point downstream of the expansion valve, as shown in Figure 1a. If the desired dew point values are above ambient temperature, the tubes connecting the output of the generator to the hygrometers are wrapped with heater tape so that they can be heated to at least 10 °C above the generated dew point temperature.

If the desired humidity values are below a frost point of −15 °C, we use the divided flow system, with the multiplexer attached to the saturator. The hygrometers are attached to the output of the multiplexer, as shown in Figure 1b.

The tubing used for connecting the generator to the hygrometers is made of electropolished stainless steel. The valves and fittings used in the manifold are also made of stainless steel. Metal-gasket face-seal fittings may be used over the entire range of the HHG. Compression fittings may be used for frostpoints and dewpoints above −40 °C.

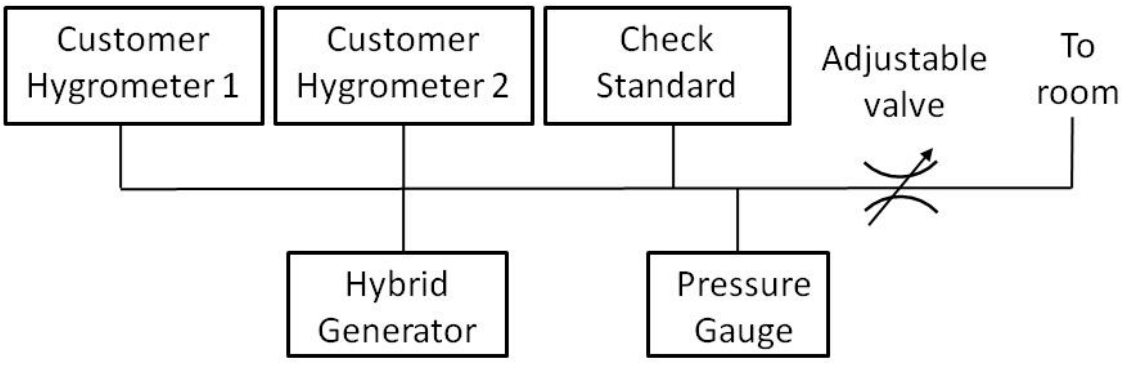

Figure 21. Connections of customer hygrometer and check standard to hybrid generator.

8.4. Data Acquisition.

The order in which the data for the calibration points is acquired is at the discretion of the operator. However, for highest efficiency we plan the order so that as many points as possible can be taken at one saturator temperature.

After setting the hybrid generator to generate the desired humidity, a computer application opens up a spreadsheet. The application then performs the data acquisition and records the measurements for the hybrid generator, check standard, and customer hygrometers in the spreadsheet at 30 s intervals for a total of 30 min. Finally, the application averages the measurements for the last 20 minutes to give the final values. If the data readings are not stable, the application is run again with the same generator parameters. If the readings are still not stable, efforts will be made to find and fix the source of the problem. The spreadsheet includes plots that monitor the saturator temperature and pressure, as well as the dew/frost point and molar fraction of the generator. It also includes plots that monitor the measurements of the check standard and customer hygrometers.

For the calibration points with the highest and lowest humidity values, the computer application is run twice to check the repeatability of the hygrometer. If the repeat measurements agree with the first measurements to within the historical repeatability for that type of hygrometer, then this historical repeatability is assigned to the customer hygrometer. If the repeat measurements do not agree, additional uncertainty is added or the hygrometer is rejected, depending on the degree of disagreement. For the case of chilled-mirror hygrometers, the dew/frost layer is removed before the repeat measurements are made so that a new dew/frost layer will form for the next data set.

After the first calibration point is completed and the hygrometer repeatability established, measurements at the subsequent calibration point are performed only once. An exception to this rule is made if the calibration measurement value is anomalous to the group of calibration points and appears suspect.

8.5. Quality Control.

If the stability and/or repeatability of the hygrometer are significantly worse than the values given by the hygrometer specifications and the sources of these problems cannot be corrected, the hygrometer is rejected for calibration and returned to the customer.

As a check on the consistency of the HHG, a check standard (a chilled-mirror hygrometer) is attached to the output of the generator as shown in Fig. 21 when performing calibrations. A measurement history of the check standard exists for dew/frost points at available multiples of 10 °C (i.e. −70 °C, −60 °C, … 70 °C, 80 °C) as well as 84 °C. During the course of a hygrometer calibration, comparisons are made of at least two check-standard points. These points are preferably at the highest and lowest customer calibration points. If the highest/lowest customer calibration points have no check-standard history, additional data is taken at the check-standard points closest to them. Data acquisition for the check standard is performed as described in section 8.4. After the check-standard data acquisition and evaluation is complete, the new check standard results are compared to earlier check standard results. If the new check

standard measurements differ from the trend line set by the old measurements by more than the expanded total uncertainty (k=2) of the HHG and hygrometer, the new results are considered suspect, and further investigation must be made to determine the validity of these results. An example of a check-standard history plot is shown in Fig. 22.

At a minimum of once every four months, cross checks are made on the pressure measurement and temperature measurement systems for the final saturator to ensure that their measurements are within the stated uncertainties. For the two pressure gauges, measurements are first performed on a vacuum to measure their zero-offset values and correct for them in the data acquisition application. Measurements are then made at ambient pressure to compare the gauges' measured values with those from a calibrated aneroid barometer. If the comparison at ambient pressure yields results that are outside of the stated uncertainty, the gauges are recalibrated against a piston gauge with a NIST-traceable calibration. For the temperature measurement system, the bath temperature measured by the SPRT is compared with that displayed by the bath control when the bath is at 20 °C to test for consistency with previous comparisons. In addition, the resistance of a second calibrated standard resistor is measured with the SPRT's resistance-measurement system to test its integrity.

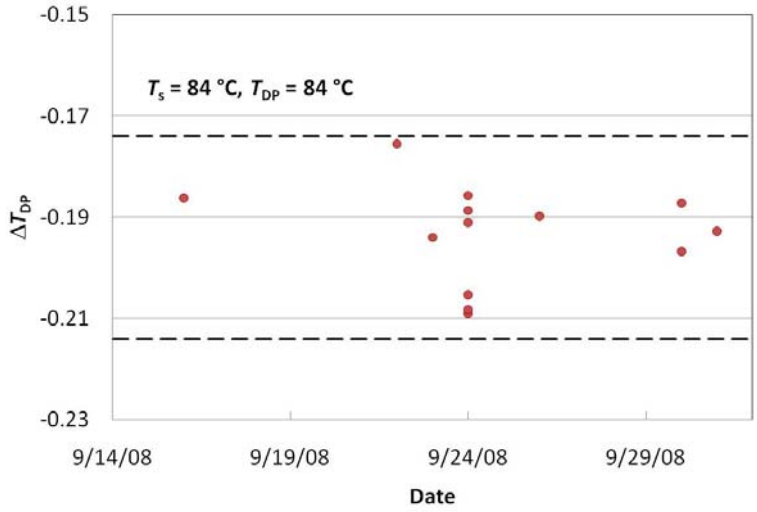

Figure 22. Check Standard history plot for a dew point of 84 °C. Here, the saturator temperature is T_s = 84 °C. The plot shows the difference ΔT_{DP} between the dew point temperature measured by the check standard and that generated by the HHG as a function of date. The dashed lines represent the k = 2 uncertainty limits for the hygrometer repeatability.

9. Summary

We have described here the design and performance of the new hybrid generator at NIST, which generates dew/frost-points between −70 °C and 85 °C (mole fractions between 2.5 μmol/mol and 0.57 mol/mol). This primary generator uses a novel design that incorporates both the two-pressure method and divided-flow method; this provides an opportunity to perform validation tests on the conventional 2-P method in the low-frost-point range. Between −60 °C and 85 °C the dew/frost-point expanded uncertainty is always below 25 mK. Between −70 °C and −60 °C the uncertainty is between 25 mK and 60 mK. Over the low frost point range, this uncertainty is considerably lower than the uncertainty of most 2-P generators, including that of NIST. Over the range −70 °C to −60 °C, the uncertainty of the HHG is larger than the uncertainties for higher ranges due to the increasing influence of the uncertainty of x_p, which we estimate to be $u(x_p) = 10$ nmol/mol. Comparison of the expected humidity generated by the HHG with that by other NIST generators shows agreement within the expanded uncertainties of the generators and transfer hygrometer. Comparison of the expected humidity generated by the HHG with that measured by the NIST gravimetric hygrometer also shows agreement within the combined expanded uncertainties of the generator and hygrometer. These comparisons provide a satisfactory validation of the performance of the HHG.

References

[1] G.E. Scace et al., An Overview of the NIST Hybrid Humidity Generator, in Proceedings of the 5th International Symposium on Humidity and Moisture (Rio de Janeiro, Brazil: INMETRO, 2007).

[2] C.W. Meyer et al, Performance and Validation Tests on the NIST Hybrid Humidity Generator, in Proceedings of the 10th International Symposium on Temperature and Thermal Measurements in Industry and Science (TEMPMEKO 2007), Int. J. Thermophys., DOI 10.1007/s10765-007-0342-4.

.

[3] A. Saul and W. Wagner, International Equations for the Saturation Properties of Ordinary Water Substance, J. Phys. Chem. Ref. Data **16,** 893−901 (1987).

[4] W. Wagner and A. Pruss, International Equations for the Saturation Properties of Ordinary Water Substance--Revised According to the International Temperature Scale of 1990, J. Phys. Chem. Ref. Data **22**, 783−787 (1993).

[5] R.W. Hyland and A. Wexler, Formulations for the Thermodynamic Properties of Dry Air from 173.15 K to 473.15 K, and of Saturated Moist Air from 173.15 K to 372.15 K, at Pressures to 5 MPa., ASHRAE Trans. **89-IIa**, 520−535 (1983).

[6] A. Wexler, Humidity Standards, Tappi **44** (6), 180A −191 A (1961).

[7] International Association for the Properties of Water and Steam, Revised Release on the Pressure along the Melting and Sublimation Curves of Ordinary Water Substance (2008), available at www.iapws.org.

[8] W. Wagner, R. Feistel, and T. Riethmann, New Equations for the Melting Pressure and Sublimation Pressure of H_2O Ice Ih. To be submitted to J. Phys. Chem. Ref. Data.

[9] International Association for the Properties of Water and Steam, Release on the Ionization Constant of H_2O (2007), available at www.iapws.org.

[10] A. Picard et al., Metrologia, **45**, 149 (2008).

[11] ASTM Standard E 1137/E 1137M - 04, Annual Book of ASTM Standards, vol. 14.03, ASTM International, Conshohocken, PA (2006), 473-479.

[12] ISO, Guide to the Expression of Uncertainty in Measurement, International Organization for Standardization, Geneva (1993).

[13] B.N. Taylor and C.E. Kuyatt, Guidelines for Evaluating and Expressing the Uncertainty of NIST Measurement Results, NIST Technical Note 1297, National Institute of Standards and Technology, Gaithersburg (1994).

[14] C.D. Vaughn and G.F. Strouse, The NIST Industrial Thermometer Calibration Laboratory, in Proceedings of TEMPMEKO 2001: the 8th International Symposium on Temperature and Thermal Measurements, B. Fellmuth, J. Seidel, G. Scholz, eds., VDE Verlag GMBH, Berlin (2002), 629-634.

[15] A. Wexler, Vapor Pressure Formulation for Water in Range 0 to 100 °C, Jour. Res. NBS **80A**, 775−785 (1976).

[16] R.W. Hyland, A Correlation for the Second Interaction Virial Coefficients and Enhancement Factors for Moist Air, Jour. Res. NBS **79A**, 551−560 (1975).

[17] S. Hasegawa and J.W. Little, The NBS Two-Pressure Humidity Generator, Mark 2, Jour. Res. NBS **81A**, 81−88 (1977).

[18] G.E. Scace and J.T. Hodges, Uncertainty of the NIST Low Frost-point Humidity Generator, in Proceedings of TEMPMEKO 2001: the 8th International Symposium on Temperature and Thermal Measurements, B. Fellmuth, J. Seidel, G. Scholz, eds., VDE Verlag GMBH, Berlin (2002), 597-602.

[19] P.H. Huang, Determining Uncertainties of Relative Humidity, Dew/frost-point Temperature, and Mixing Ratio in a Humidity Standard Generator, in Papers and Abstracts from the Third International Symposium on Humidity and Moisture, National Physical Laboratory, Teddington, UK (1998), 149-158.

[20] J.W. Lovell-Smith, On Correlation in the Water Vapour Pressure Formulation, Metrologia **43**, 556-560 (2006).

[21] C.W. Meyer et al., Automated Continuous-Flow Gravimetric Hygrometer as a Primary Humidity Standard, in Proceedings of the 5th International Symposium on Humidity and Moisture, (Rio de Janeiro, Brazil: INMETRO, 2007).

[22] C.W. Meyer et al., A Second-Generation NIST Gravimetric Hygrometer, in preparation.

Appendix I. Derivation of the Uncertainty Equations for the Hybrid Generator

The total uncertainty of a quantity z is related to the n individual uncertainty components y_i through the general law of error propagation [12]:

$$u(z)^2 = \sum_{i=1}^{n}\left(\frac{\partial z}{\partial y_i}\right)u(y_i)^2 + 2\sum_{i=1}^{n-1}\sum_{j=i+1}^{n} r_{i,j}\frac{\partial z}{\partial y_i}\frac{\partial z}{\partial y_j}u(y_i)\,u(y_j) \qquad \text{A1)}$$

The relevant quantities and the derivatives $\partial z/\partial y_i$ may be found by expanding the differential dz:

$$dz = \sum_{i=1}^{n}\frac{\partial z}{\partial y_i}dy_i \ . \qquad \text{A2)}$$

Below, the total uncertainty for humidity generated by the hybrid generator will be derived for four cases: 1) water mole fraction when the generator is used in 2-P mode or 1-P mode, 2) dew-point temperature when the generator is used in 2-P mode or 1-P mode, 3) water mole fraction when the generator is used in divided-flow mode, and 4) frost-point temperature when the generator is used in divided-flow mode.

1. Water Mole Fraction When the Generator is Used in 2-P Mode or 1-P Mode

The total uncertainty for this case is obtained by applying Eq. A2 to Eq. 1, which yields

$$dx = \frac{f_s}{P_s}de_s + \frac{e_s}{P_s}df_s - \frac{e_s f_s}{P_s^{\,2}}dP_s \ . \qquad \text{A3)}$$

where $f_s \equiv f(T_s,P_s)$ and $e_s \equiv e\,(T_s,P_s)$. In de_s, we can separate out the differential relating to the uncertainty of its calculating equation de_s^{calc} from that relating to the uncertainty of the temperature from which it is calculated:

$$de_s = de_s^{calc} + \frac{de_s}{dT_s}dT_s \ . \qquad \text{A4)}$$

Similarly, in df_s, we can separate out to the differential relating to the uncertainty of its calculating equation df_s^{calc} from that relating to the uncertainty of the temperature and pressure from which it is calculated:

$$df_s = df_s^{calc} + \frac{df_s}{dT_s}dT_s + \frac{df_s}{dP_s}dP_s \ . \qquad \text{A5)}$$

However, because $f_s \approx 1$, df_s/dT_s and df_s/dP_s are very small and so Eq. A5 may be approximated as $df_s \approx df_s^{calc}$. Using these two approximations while combining Eqs. A3−A4 gives

$$dx = \frac{1}{P_s}\frac{de_s}{dT_s}dT_s - \frac{e_s}{P_s^{\,2}}dP_s + \frac{1}{P_s}de_s^{\,\mathrm{calc}} + \frac{e_s}{P_s}df_s^{\,\mathrm{calc}}. \qquad \text{A6)}$$

The uncertainty in the mole fraction may then be expressed as

$$u(x)^2 = \left(\frac{1}{P_s}\frac{de_s}{dT_s}\right)^2 u(T_s)^2 + \left(\frac{e_s}{P_s^{\,2}}\right)^2 u(P_s)^2 + \left(\frac{1}{P_s}\right)^2 u\left(e_s^{\,\mathrm{calc}}\right)^2 + \left(\frac{e_s}{P_s}\right)^2 u\left(f_s^{\,\mathrm{calc}}\right)^2. \qquad \text{A7)}$$

2. Dew-point Temperature When the Generator is Used in 2-P Mode or 1-P Mode

Here we consider the total uncertainty for the dew point temperature T_{DP} in a chamber with temperature $T_c = T_{DP}$, pressure P_c, and water vapor pressure e_c. This uncertainty may be determined by inverting Eq. A4 to solve for dT_s and then substituting the saturator parameters with the chamber parameters (T_s with T_{DP}, e_s with e_c, and $e_s^{\,\mathrm{calc}}$ with $e_c^{\,\mathrm{calc}}$):

$$dT_{DP} = dT_c = \frac{1}{\left[de_c / dT_{DP}\right]}\left(de_c - de_c^{\,\mathrm{calc}}\right). \qquad \text{A8)}$$

Letting $f_c \equiv f(T_c, P_c)$, we can express e_c in terms of x and P_c:

$$e_c = \frac{xP_c}{f_c}. \qquad \text{A9)}$$

Differentiating Eq. A9 and inserting the resulting expression for de_c in Eq. A8 gives

$$dT_{DP} = \frac{1}{\left[de_c / dT_{DP}\right]}\left[\frac{P_c}{f_c}dx + \frac{x}{f_c}dP_c - \frac{xP_c}{f_c^{\,2}}df_c - de_c^{\,\mathrm{calc}}\right]. \qquad \text{A10)}$$

Using the approximations $f_c \cong 1$ and $df_c \cong df_c^{\,\mathrm{calc}}$ in Eq. A10 and combining it with Eqs. 1 and A6 and yields

$$dT_{DP} = \frac{1}{\left[de_c / dT_c\right]}\left[\frac{P_c}{P_s}\frac{de_s}{dT_s}dT_s - \frac{P_c e_s}{P_s^{\,2}}dP_s + \left(\frac{P_c}{P_s}de_s^{\,\mathrm{calc}} - de_c^{\,\mathrm{calc}}\right) + e_c\left(df_s^{\,\mathrm{calc}} - df_c^{\,\mathrm{calc}}\right) + \frac{e_c}{P_c}dP_c\right]. \qquad \text{A11)}$$

Recognizing that x is the same in both the saturator and chamber, $e_s / P_s \cong e_c / P_c$, and so A11 may be written

$$dT_{\mathrm{DP}} = \frac{e_{\mathrm{c}}}{\left[de_{\mathrm{c}} / dT_{\mathrm{DP}}\right]}\left[\frac{1}{e_{\mathrm{s}}}\frac{de_{\mathrm{s}}}{dT_{\mathrm{s}}}dT_{\mathrm{s}} - \frac{dP_{\mathrm{s}}}{P_{\mathrm{s}}} + \left(\frac{de_{\mathrm{s}}^{\mathrm{calc}}}{e_{\mathrm{s}}} - \frac{de_{\mathrm{c}}^{\mathrm{calc}}}{e_{\mathrm{c}}}\right) + \left(df_{\mathrm{s}}^{\mathrm{calc}} - df_{\mathrm{c}}^{\mathrm{calc}}\right) + \frac{dP_{\mathrm{c}}}{P_{\mathrm{c}}}\right]. \quad \text{A12)}$$

This equation can be simplified by defining the differentials

$$d\Delta e^{\mathrm{calc}} \equiv \frac{de_{\mathrm{s}}^{\mathrm{calc}}}{e_{\mathrm{s}}} - \frac{de_{\mathrm{c}}^{\mathrm{calc}}}{e_{\mathrm{c}}} \quad \text{and} \quad \text{A13)}$$

$$d\Delta f^{\mathrm{calc}} \equiv df_{\mathrm{s}}^{\mathrm{calc}} - df_{\mathrm{c}}^{\mathrm{calc}}. \quad \text{A14)}$$

Then Eq. A12 becomes

$$dT_{\mathrm{DP}} = \frac{e_{\mathrm{c}}}{\left[de_{\mathrm{c}} / dT_{\mathrm{DP}}\right]}\left[\frac{1}{e_{\mathrm{s}}}\frac{de_{\mathrm{s}}}{dT_{\mathrm{s}}}dT_{\mathrm{s}} - \frac{dP_{\mathrm{s}}}{P_{\mathrm{s}}} + d\Delta e^{\mathrm{calc}} + d\Delta f^{\mathrm{calc}} + \frac{dP_{\mathrm{c}}}{P_{\mathrm{c}}}\right]. \quad \text{A15)}$$

And the uncertainty of the dew point temperature is

$$u\left(T_{\mathrm{DP}}\right)^2 = \left(\frac{e_{\mathrm{c}}}{\left[de_{\mathrm{c}} / dT_{\mathrm{DP}}\right]}\right)^2\left[\left(\frac{1}{e_{\mathrm{s}}}\frac{de_{\mathrm{s}}}{dT_{\mathrm{s}}}\right)^2 u\left(T_{\mathrm{s}}\right)^2 + \frac{u\left(P_{\mathrm{s}}\right)^2}{P_{\mathrm{s}}{}^2} + \frac{u\left(P_{\mathrm{c}}\right)^2}{P_{\mathrm{c}}{}^2} + u\left(\Delta f^{\mathrm{calc}}\right)^2 + u\left(\Delta e_{\mathrm{r}}^{\mathrm{calc}}\right)^2\right] \quad \text{A16)}$$

The uncertainties $u\left(\Delta f^{\mathrm{calc}}\right)$ and $u\left(\Delta e^{\mathrm{calc}}\right)$ have not been resolved by the humidity community, and it is currently an area of active work [20]. Because of this, we use in this document the conventional analysis [20]. When the generator is used in 1-P mode ($P_{\mathrm{s}} \cong P_{\mathrm{c}}$), this method assumes that $e_{\mathrm{c}} \cong e_{\mathrm{s}}$ and $f_{\mathrm{c}} \cong f_{\mathrm{s}}$, and therefore

$$u\left(\Delta e_{\mathrm{r}}^{\mathrm{calc}}\right) = u\left(\Delta f^{\mathrm{calc}}\right) = 0 \quad \text{A17)}$$

For the 2-P mode ($P_{\mathrm{s}} \neq P_{\mathrm{c}}$), the method assumes that there are no correlations between $u\left(e_{\mathrm{s}}^{\mathrm{calc}}\right)$ and $u\left(e_{\mathrm{c}}^{\mathrm{calc}}\right)$ and between $u\left(f_{\mathrm{s}}^{\mathrm{calc}}\right)$ and $u\left(f_{\mathrm{c}}^{\mathrm{calc}}\right)$; therefore

$$u\left(\Delta e_{\mathrm{r}}^{\mathrm{calc}}\right)^2 \equiv \frac{u\left(e_{\mathrm{s}}^{\mathrm{calc}}\right)^2}{e_{\mathrm{s}}{}^2} + \frac{u\left(e_{\mathrm{c}}^{\mathrm{calc}}\right)^2}{e_{\mathrm{c}}{}^2} \quad \text{and} \quad \text{A18)}$$

$$u\left(\Delta f^{\mathrm{calc}}\right)^2 \equiv u\left(f_{\mathrm{s}}^{\mathrm{calc}}\right)^2 + u\left(f_{\mathrm{c}}^{\mathrm{calc}}\right)^2. \quad \text{A19)}$$

3. Relative Humidity When the Generator is Used in 2-P Mode or 1-P Mode

Here we consider the total uncertainty for the relative humidity *RH* in a chamber with temperature T_c, pressure P_c when the generator is used in 2-P or 1-P mode. The relative humidity is defined as

$$RH \equiv \frac{e_p}{e_c}, \tag{A20}$$

where the partial water vapor pressure e_p in the chamber is given by

$$e_p = \frac{xP_c}{f_c} \tag{A21}$$

and e_c is the saturated water vapor pressure for the chamber at temperature T_c. Note that e_c is a function of T_c, while e_p is an independent variable. Placing Eq. A21 into Eq. A20,

$$RH \equiv \frac{xP_c}{e_c f_c} = \frac{e_s f_s P_c}{e_c f_c P_s}, \tag{A22}$$

The total uncertainty for this case is obtained by applying Eq. A2 to Eq. A21, which yields

$$d(RH) = \frac{f_s P_c}{e_c f_c P_s} de_s + \frac{e_s P_c}{e_c f_c P_s} df_s + \frac{e_s f_s}{e_c f_c P_s} dP_c - \frac{e_s f_s P_c}{e_c f_c^2 P_s} df_c - \frac{e_s f_s P_c}{e_c f_c P_s^2} dP_s - \frac{e_s f_s P_c}{e_c^2 f_c P_s} de_c. \tag{A23}$$

Recognizing that

$$de = de^{calc} + \frac{de}{dT} dT \tag{A24}$$

and by approximating $f_s = f_c \cong 1$, A22 becomes

$$\begin{aligned} d(RH) = {} & \frac{P_c}{P_s e_c}\left[de_s^{calc} + \frac{de_s}{dT_s} dT_s \right] + \frac{e_s P_c}{P_s e_c} df_s + \frac{e_s}{P_s e_c} dP_c \\ & - \frac{e_s P_c}{e_c P_s} df_c - \frac{e_s P_c}{e_c P_s^2} dP_s - \frac{e_s P_c}{e_c^2 P_s}\left[de_c^{calc} + \frac{de_c}{dT_c} dT_c \right] \end{aligned}. \tag{A25}$$

Inserting Eqs. A13 and A14 yields:

$$d(RH) = \frac{P_c}{P_s e_c}\frac{de_s}{dT_s}dT_s + \frac{e_s}{P_s e_c}dP_c - \frac{e_s P_c}{e_c P_s^{\,2}}dP_s - \frac{e_s P_c}{e_c^{\,2} P_s}\frac{de_c}{dT_c}dT_c + \frac{e_s P_c}{e_c P_s}\frac{de_c}{dT_c}d\Delta e^{\text{calc}} + \frac{e_s P_c}{e_c P_s}d\Delta f$$
$$= \frac{P_c e_s}{P_s e_c}\left[\frac{1}{e_s}\frac{de_s}{dT_s}dT_s + \frac{dP_c}{P_c} - \frac{dP_s}{P_s} - \frac{1}{e_c}\frac{de_c}{dT_c}dT_c + d\Delta e^{\text{calc}} + d\Delta f\right] \quad \text{A26)}$$

Remembering $e_s / P_s \cong e_c / P_c$, the uncertainty for the relative humidity is then

$$u(RH)^2 = \left[\left(\frac{1}{e_s}\frac{de_s}{dT_s}\right)^2 u(T_s)^2 + \frac{1}{P_c^{\,2}}u(P_c)^2 + \frac{1}{P_s^{\,2}}u(P_s)^2 + \left(\frac{1}{e_c}\frac{de_c}{dT_c}\right)^2 u(T_c)^2 + u\left(\Delta e^{\text{calc}}\right)^2 + u\left(\Delta f^{\text{calc}}\right)^2\right] \quad \text{A27)}$$

Once again, the values of $u\left(\Delta e^{\text{calc}}\right)$ and $u\left(\Delta f^{\text{calc}}\right)$ are best estimated by Eq. A16 when the generator is used in 1-P mode and by Eq. A17 and Eq. A18 when the generator is used in 2-P mode.

4. Water Mole Fraction When the Generator is Used in Divided-flow Mode

For the generator used with the divided-flow method, the differential for the mole fraction may be expanded as

$$dx = \frac{\dot{n}_s\, dx_s + \dot{n}_p\, dx_p}{\dot{N}} + \frac{\dot{n}_p\left(x_s - x_p\right)}{\dot{N}^2}d\dot{n}_s - \frac{\dot{n}_s\left(x_s - x_p\right)}{\dot{N}^2}d\dot{n}_p \quad \text{A28)}$$

Since $x_p \ll x_s$, this reduces to

$$dx \cong \frac{\dot{n}_s}{\dot{N}}dx_s + \frac{\dot{n}_p}{\dot{N}}dx_p + \frac{\dot{n}_p x_s}{\dot{N}^2}d\dot{n}_s - \frac{\dot{n}_s x_s}{\dot{N}^2}d\dot{n}_p \quad \text{A29)}$$

Using the result of Eq. A6 as dx_s, and noting $x_s \cong e_s / P_s$, this becomes

$$dx \cong \frac{\dot{n}_s}{\dot{N}P_s}\frac{de_s}{dT_s}dT_s - \frac{\dot{n}_s e_s}{\dot{N}P_s^{\,2}}dP_s + \frac{\dot{n}_s}{\dot{N}P_s}de_s^{\text{calc}} + \frac{\dot{n}_s e_s}{\dot{N}P_s}df_s^{\text{calc}} + \frac{\dot{n}_p}{\dot{N}}dx_p + \frac{\dot{n}_p e_s}{\dot{N}^2 P_s}d\dot{n}_s - \frac{\dot{n}_s e_s}{\dot{N}^2 P_s}d\dot{n}_p \quad \text{A30)}$$

Noting that $x \cong \dot{n}_s e_s / \dot{N}P_s$ and $x_s \cong e_s / P_s$, the mole fraction uncertainty is then

$$u(x)^2 \cong x^2\left[\left(\frac{1}{e_s}\frac{de_s}{dT_s}\right)^2 u(T_s)^2 + \frac{u(P_s)^2}{P_s{}^2} + \frac{u\left(e_s^{\text{calc}}\right)^2}{e_s{}^2} + u\left(f_s{}^{\text{calc}}\right)^2 + \frac{u(\dot{n}_p)^2}{\dot{N}^2} + \left(\frac{x_s}{x}-1\right)^2\left(\frac{u(x_p)^2}{x_s{}^2} + \frac{u(\dot{n}_s)^2}{\dot{N}^2}\right)\right] \quad \text{A31)}$$

5. Frost-point Temperature When the Generator is Used in Divided-flow Mode

In the hybrid generator, the divided flow method will only be used for generating frost points. We expand the frost-point temperature differential by combining Eqs. A10 and A30, which yields

$$dT_{FP} = \frac{P_c}{\left[de_c/dT_c\right]}\left[\frac{\dot{n}_s}{\dot{N}P_s}\frac{de_s}{dT_s}dT_s - \frac{\dot{n}_s e_s}{\dot{N}P_s{}^2}dP_s + \frac{\dot{n}_s}{\dot{N}P_s}de_s^{\text{calc}} + \frac{\dot{n}_s e_s}{\dot{N}P_s}df_s{}^{\text{calc}} + \frac{\dot{n}_p}{\dot{N}}dx_p + \frac{\dot{n}_p e_s}{\dot{N}^2 P_s}d\dot{n}_s + \frac{\dot{n}_s e_s}{\dot{N}^2 P_s}d\dot{n}_p + xd - xdf_c{}^{\text{calc}} - \frac{1}{P_c}de_c^{\text{calc}}\right] . \quad \text{A32)}$$

Here e_c is the saturated vapor pressure for ice. Because of this, we assume no correlation between the uncertainties of e_c^{calc} and e_s^{calc}, since e_s^{calc} is the calculation of the saturated vapor pressure for water and is different for that of ice. Using the definition for Δf^{calc} in Eq. A14, and noting that $x \cong \dot{n}_s e_s / \dot{N} P_s$ and $x_s \cong e_s / P_s$, Eq. A32 becomes

$$dT_{FP} = \frac{xP_c}{\left[de_c/dT_c\right]}\left[\frac{1}{e_s}\frac{de_s}{dT_s}dT_s - \frac{dP_s}{P_s} + \left(\frac{x_s}{x}-1\right)\left(\frac{dx_p}{x_s} + \frac{d\dot{n}_s}{\dot{N}}\right) + \frac{d\dot{n}_p}{\dot{N}} + \frac{dP_c}{P_c} + \frac{de_s^{\text{calc}}}{e_s} - \frac{de_c^{\text{calc}}}{xP_c} + d\Delta f^{\text{calc}}\right] \quad \text{A33)}$$

The frost-point temperature uncertainty then becomes

$$u(T_{FP})^2 = \frac{(xP_c)^2}{\left[de_c/dT_c\right]^2}\left[\left(\frac{1}{e_s}\frac{de_s}{dT_s}\right)^2 u(T_s)^2 + \frac{u(P_s)^2}{P_s{}^2} + \left(\frac{x_s}{x}-1\right)^2\left(\frac{u(x_p)^2}{x_s{}^2} + \frac{u(\dot{n}_s)^2}{\dot{N}^2}\right) + \frac{u(\dot{n}_p)^2}{\dot{N}^2} + \frac{u(P_c)^2}{P_c{}^2} + \frac{u\left(e_s^{\text{calc}}\right)^2}{e_s{}^2} + \frac{u\left(e_c^{\text{calc}}\right)^2}{(xP_c)^2} + u\left(\Delta f^{\text{calc}}\right)^2\right] \quad \text{A34)}$$

Here, we once again use the conventional method for estimating $u\left(\Delta f^{\text{calc}}\right)^2$, which employs Eq. A18.

6. Relative Humidity When the Generator is Used in Divided-flow Mode

Here we consider the total uncertainty for the relative humidity *RH* in a chamber with temperature T_c and pressure P_c when the generator is used in divided-flow mode. From Eqs. A20-A22, the relative humidity is

$$RH \equiv \frac{xP_c}{e_c f_c}, \tag{A35}$$

and so

$$d(RH) = \frac{P_c}{e_c f_c}dx + \frac{x}{e_c f_c}dP_c - \frac{xP_c}{e_c^{\,2} f_c}de_c - \frac{xP_c}{e_c f_c^{\,2}}df_c \tag{A36}$$

Inserting Eq. 6, Eq. A24, and Eq. A30 and into Eq. A36 yields:

$$\begin{aligned} d(RH) = \frac{xP_c}{e_c}\left[\frac{1}{e_s}\frac{de_s}{dT_s}dT_s - \frac{dP_s}{P_s} + \frac{de_s^{\,\mathrm{calc}}}{e_s} + df_s^{\,\mathrm{calc}} + \left(\frac{x_s}{x}-1\right)\left(\frac{dx_p}{x_s} + \frac{d\dot{n}_s}{\dot{N}}\right) - \frac{d\dot{n}_p}{\dot{N}}\right] \\ + \left(\frac{P_c}{e_c}\right)\left(x + \frac{\dot{n}_p}{\dot{N}}x_p\right)\left(\frac{dP_c}{P_c} - \frac{1}{e_c}\frac{de_c}{dT_c}dT_c - \frac{1}{e_c}de_c^{\,\mathrm{calc}} - df_c\right) \end{aligned} \tag{A37}$$

The uncertainty for relative humidity is then:

$$\begin{aligned} u(RH)^2 = \left[\frac{xP_c}{e_c}\right]^2\Bigg[\left(\frac{1}{e_s}\frac{de_s}{dT_s}\right)^2 u(T_s)^2 + \frac{u(P_s)^2}{P_s^{\,2}} + \frac{u\left(e_s^{\,\mathrm{calc}}\right)^2}{e_s^{\,2}} \\ + u\left(f_s^{\,\mathrm{calc}}\right)^2 + \left(\frac{x_s}{x}-1\right)^2\left(\frac{u(x_p)^2}{x_s^{\,2}} + \frac{u(\dot{n}_s)^2}{\dot{N}^2}\right) + \frac{u(\dot{n}_p)^2}{\dot{N}^2}\Bigg] \\ + \left(\frac{P_c}{e_c}\right)^2\left(x + \frac{\dot{n}_p}{\dot{N}}x_p\right)^2\left[\frac{u(P_c)^2}{P_c^{\,2}} + \left(\frac{1}{e_c}\frac{de_c}{dT_c}\right)^2 u(T_c)^2 + \frac{u(e_c^{\,\mathrm{calc}})^2}{e_c^{\,2}} + u(f_c^{\,\mathrm{calc}})^2\right] \end{aligned} \tag{38}$$

Appendix II. Uncertainty Element Subcomponents for the Hybrid Generator

Table 2. Subcomponents for the uncertainty elements T_s, P_s, and P_c

	Source of uncertainty		**Standard Uncertainty**	**Unit**
Saturator Temperature T_s	*Saturator*	Saturation efficiency	0.5	mK
		Bath gradients	1 ($T \leq 40$ °C) $0.16T$/°C – 5.4 ($T > 40$ °C)	mK
		Air contamination	< 0.2	mK
		Water contamination	< 0.2	mK
		Stability	1	mK
	SPRT	Calibration	0.5	mK
		Drift	0.3	mK
		Self-heating	0.1	mK
	Bridge	Calibration	0.1	mK
		Resolution	0.1	mK
Saturator Pressure P_s	*Pressure gauge*	Calibration	7	Pa
		Drift	$10 + 0.0001\ P_s$/Pa	Pa
		Resolution	7	Pa
		Hydrostatic head	1	Pa
		Flow effect	2	Pa
		Repeatability	7	Pa
	Throttle Valve	P_s stability	7 ($P_s \approx$ ambient pressure) 20 ($P_s >$ ambient pressure)	Pa
Chamber Pressure P_c	*Pressure gauge*	Calibration	7	Pa
		Drift	5	Pa
		Resolution	7	Pa
		Hydrostatic head	1	Pa
		Flow effect	2	Pa
		Repeatability	7	Pa
		P_c stability	7	Pa

Sample Calibration Report

UNITED STATES DEPARTMENT OF COMMERCE
NATIONAL INSTITUTE OF STANDARDS AND TECHNOLOGY
GAITHERSBURG, MARYLAND

REPORT OF CALIBRATION
DEW-POINT HYGROMETER

DPH Systems S/N 28637

Submitted by

Humidity Measurement Instruments
Peoria, IL 61615

The dew-point hygrometer was calibrated by comparison against air of known moisture content, generated by the NIST Hybrid Humidity Generator. The hygrometer mirror was cleaned using ethanol before the calibration. Subsequently, the outlet from the generator was connected to the inlet of the hygrometer using a 1/4-inch (0.635) diameter stainless steel tube. The dew points generated during the calibration ranged from −70 °C to 20 °C. For each calibration point, the following procedure was used. The generator was set to produce humidified air with a flow of 30 standard liters per minute (SLM), and 0.5 SLM of this air was set to pass through the hygrometer. Once the flow started, humidity measurements were made with the hygrometer to determine when the readings reached a steady state. Once a steady state was reached, the determined values of the generated humidity were averaged over a period of 20 minutes, as were the values of the humidity on the hygrometer display. These average values are presented below in Table 1 for all calibration points. A minimum of six calibration data sets was taken for the first calibration point for the determination of the repeatability of the hygrometer. The standard uncertainty due to repeatability, as represented by the standard deviation of the final values of these data sets, was determined to be 0.02 °C. The generator and the complete calibration procedure are described in NIST SP250-xx, entitled "Calibration of Hygrometers with the Hybrid Humidity Generator", which may be found at http://ts.nist.gov/MeasurementServices/Calibrations/upload/SP250-xx.pdf.

The uncertainty of the calibration includes the uncertainty of the moisture content of the gas generated by the Hybrid Humidity Generator and that due to the measurement repeatability of the hygrometer. The uncertainty is expressed as an expanded relative uncertainty $U = ku_c$, with U determined from a combined standard uncertainty u_c and a coverage factor $k = 2$. The values of U are dependent on the individual calibration parameters. A discussion of the uncertainty components for the calibration and a presentation of the total uncertainties as a function of the calibration parameters is provided in NIST SP250-xx. Values of U are provided in Table 1 for each calibration point.

Measurements and analysis performed by:
Peter Huang

For the Director
National Institute of Standards and Technology

Dr. Dean Ripple
Leader, Thermometry Group
Process Measurements Division

Test No. 274-999
Measurements performed on September 20, 2007
Service ID: 36070S
Report Date: September 21, 2007

Table 1

Humidity Measurement Instruments Dew-point Hygrometer
DPH Systems S/N 28637

Dew/frost-point Temperature [°C]	**S/N 28637 Reading [°C]**	***U*** **(*k* = 2) [°C]**
20.05	19.87	0.02
10.02	10.12	0.02
0.03	0.03	0.02
−10.01	−10.11	0.03
−20.02	−20.00	0.03
−29.96	−30.01	0.03
−39.99	−40.12	0.04
−49.95	−50.14	0.04
−59.95	−60.09	0.04
−70.00	−70.14	0.05